Reactivity and Role of $SO_5^{\bullet-}$ Radical in Aqueous Medium Chain Oxidation of Sulfite to Sulfate and Atmospheric Sulfuric Acid Generation

Tomi Nath Das†

Radiation Chemistry & Chemical Dynamics Division, Bhabha Atomic Research Centre, Trombay, Mumbai 400 085, India

Received: April 4, 2001; In Final Form: July 12, 2001

This study reevaluates the role of peroxymonosulfate anion radical ($^-O_3SOO^\bullet$ or $SO_5^{\bullet-}$) intermediate during radical-induced chain oxidation of HSO_3^-/SO_3^{2-} in oxygenated aqueous solution. The $SO_5^{\bullet-}$ radical absorption band in the UV is weak: $\epsilon = 1065 \pm 80$ M^{-1} cm^{-1} at λ_{max} (260−265 nm). The $SO_5^{\bullet-}$ radical takes part in two radical−radical and four radical−solute reactions, partially producing the other chain carrier, the $SO_4^{\bullet-}$ radical, in either case. In this study, employing the pulse-radiolysis technique but adopting a new approach, these two types of reactions of the $SO_5^{\bullet-}$ radical have been separately quantified (at room temperature). For example, over pH 3.5−12, the branching ratio of ($SO_5^{\bullet-} + SO_5^{\bullet-}$) reactions giving rise to either the $SO_4^{\bullet-}$ radical or $S_2O_8^{2-}$ is found to remain ∼1. The respective reaction rate constants for $I \rightarrow 0$ are (2.2 ± 0.3) and (2.1 ± 0.3) × 10^8 M^{-1} s^{-1}. The ($SO_5^{\bullet-} + HSO_3^-$) reactions in acid pH follow two paths, forming the $SO_4^{\bullet-}$ radical in one and regenerating the $SO_3^{\bullet-}$ radical in the other, with respective rates of ca. (6.0 ± 0.4) and (3.0 ± 0.3) × 10^7 M^{-1} s^{-1}. In alkaline pH (for $SO_5^{\bullet-} + SO_3^{2-}$ reactions), the rates for similar reactions are ca. (5.6 ± 0.6) and (1.0 ± 0.1) × 10^8 M^{-1} s^{-1}. From only these results, the earlier prediction of chain length reaching a few thousands could be supported in simulation studies (Bigelow, S. L. *Z. Phys. Chem.* **1898**, *28*, 493. Young, S. W. *J. Am. Chem. Soc.* **1902**, *24*, 297. Titoff, A. *Z. Phys. Chem.* **1903**, *45*, 641. Bäckström, H. L. J. *J. Am. Chem. Soc.* **1927**, *49*, 1460. Alyea, H. N.; Bäckström, H. L. J. *J. Am. Chem. Soc.* **1929**, *51*, 90). To explore the feasibility of controlling S(IV) chain oxidation to sulfuric acid in liquid hydrometeors, the effect of radical scavenging on each $SO_x^{\bullet-}$ radical ($x = 3, 4, 5$) was simulated. The results show that for the $SO_5^{\bullet-}$ radical a scavenger reactivity of ∼100 s^{-1} may be enough to reduce the chain length by >98%. However, in the case $SO_4^{\bullet-}$ radical scavenging under similar conditions, only ∼75−80% reduction in acid production was observed. These results suggest a fresh modeling of sulfuric acid generation in atmospheric liquid hydrometeors.

Introduction

Oxygenated aqueous solution of HSO_3^-/SO_3^{2-} is known to undergo an autoxidation (chain) reaction to form sulfuric acid (i.e., mainly HSO_4^-/SO_4^{2-}).[1] The chain is initiated by free-radical oxidants including metal ions, by UV light, or even as a result of thermal oxidation.[2]

The simplified reaction Scheme 1 also represents the possible radical-induced oxidative transformations of SO_2 in atmospheric liquid hydrometeors.[3−6] In this scheme the $SO_3^{\bullet-}$ radical is first produced from HSO_3^-/SO_3^{2-} by an H-atom or electron transfer mechanism. The peroxymonosulfate anion radical ($^-O_3SOO^\bullet$ or $SO_5^{\bullet-}$) in reaction 1 is subsequently formed by O_2 attachment to $SO_3^{\bullet-}$ radical. Postulated $SO_5^{\bullet-}$ radical reactions are eqs 2−5.[2]

$$SO_3^{\bullet-} + O_2 \rightarrow SO_5^{\bullet-} \quad (1)$$

$$SO_5^{\bullet-} + SO_5^{\bullet-} \rightarrow 2SO_4^{\bullet-} + O_2 \quad (2)$$

$$SO_5^{\bullet-} + HSO_3^-/SO_3^{2-} \rightarrow SO_4^{\bullet-} + SO_4^{2-} (+H_3O^+) \quad (3)$$

$$SO_5^{\bullet-} + HSO_3^-/SO_3^{2-} \rightarrow HSO_5^-/SO_5^{2-} + SO_3^{\bullet-} \quad (4)$$

$$SO_5^{\bullet-} + SO_5^{\bullet-} \rightarrow S_2O_8^{2-} + O_2 \quad (5)$$

While one part generates $SO_4^{\bullet-}$ radical by radical dimerization−elimination in reaction 2 and O-atom transfer to excess S(IV) in reaction 3, another fraction regenerates the $SO_3^{\bullet-}$ radical either by H-atom or electron transfer, reaction 4, to propagate the chain. The remaining $SO_5^{\bullet-}$ radicals take part in reaction 5, which may temporarily be considered as a chain-exit reaction in Scheme 1. In the atmosphere, in addition to these six primary reactions, $SO_5^{\bullet-}$ radical scavenging by dissolved impurities may open up additional reaction pathways and influence the chain length.

SCHEME 1

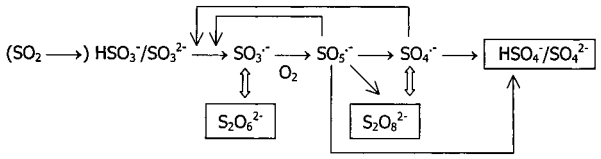

The other related set of reactions include the $SO_4^{\bullet-}$ radical reduction to form sulfate anion (i.e., sulfuric acid) following mainly reaction 6 or dimerization following reaction 7.

$$SO_4^{\bullet-} + HSO_3^-/SO_3^{2-} \rightarrow SO_3^{\bullet-} + SO_4^{2-} (+H^+) \quad (6)$$

$$SO_4^{\bullet-} + SO_4^{\bullet-} \rightarrow S_2O_8^{2-} \quad (7)$$

Sustenance of the oxidative chain is feasible as long as reactions 3, 4, and 6 have higher propensities over reactions 5 and 7 or other radical-loss processes. Of course, under favorable circumstances, $S_2O_8^{2-}$ can regenerate the $SO_4^{\bullet-}$ radical as a result of photolysis just as any $S_2O_6^{2-}$ produced from $SO_3^{\bullet-}$ radical dimerization can also decompose to regenerate the $SO_3^{\bullet-}$ radical. However, these two reactions may not actively partici-

† Fax: 91-22-5505151. E-mail: tndas@apsara.barc.ernet.in.

10.1021/jp011255h CCC: $20.00
Published on Web 09/14/2001

TABLE 1: Reported Reaction Kinetics of $SO_5^{\bullet-}$ Radical

reactions	ref = rate constant (M^{-1} s^{-1})[a]
$SO_5^{\bullet-} + SO_5^{\bullet-} \rightarrow 2SO_4^{\bullet-} + O_2$	$16 = 5.2 \times 10^6$; $15 = 8.7 \times 10^7$; $13 < 1.0 \times 10^8$; $12 < 2.0 \times 10^8$; $17 = 2.0 \times 10^8$; $10 = 2.2 \times 10^8$; 6, 11, $14 = 6.0 \times 10^8$; $5 = 8.4 \times 10^6$
$SO_5^{\bullet-} + SO_5^{\bullet-} \rightarrow S_2O_8^{2-} + O_2$	$15 = 1.4 \times 10^7$; $10 = 4.8 \times 10^7$; $13 < 1.0 \times 10^8$; $16 = 1.2 \times 10^8$; 5, 6, 11, & $14 = 1.4 \times 10^8$; $9 = (1.0-1.5) \times 10^8$
$SO_5^{\bullet-} + HSO_3^- \rightarrow HSO_4^- + SO_4^{\bullet-}$	$10 = 3.6 \times 10^2$; $5 = 2.5 \times 10^4$; $11 < 3.0 \times 10^5$
$SO_5^{\bullet-} + SO_3^{2-} \rightarrow HSO_4^- + SO_4^{\bullet-}$	$11 = 7.5 \times 10^4$; $10 = 5.5 \times 10^6$; $5 = 9.0 \times 10^6$; $14 \approx 1.0 \times 10^7$
$SO_5^{\bullet-} + HSO_3^- \rightarrow HSO_5^- + SO_3^{\bullet-}$	$10 = 8.6 \times 10^3$; $5 = 7.5 \times 10^4$; $11 < 3.0 \times 10^5$
$SO_5^{\bullet-} + SO_3^{2-} \rightarrow HSO_5^- + SO_3^{\bullet-}$	$11 = 2.5 \times 10^4$; $10 = 2.1 \times 10^5$; $14 = 3.0 \times 10^6$; $5 = 3.8 \times 10^6$

[a] As measured, reported, or used in previous studies.

pate in the time scale of the chain oxidation process. In Scheme 1, the efficiency of O_2 replenishment at the reaction zone is also expected to influence the chain length, especially at very high S(IV) concentrations. Chain lengths of hundreds to thousands in laboratory studies[1] suggest that the atmosphere aqueous medium oxidation of SO_2 may dominate over its gas phase reactions to generate sulfuric acid and possibly introduce additional sulfur−oxygen species such as $S_2O_6^{2-}$, $S_2O_8^{2-}$, and HSO_5^{2-}/SO_5^{2-} into the atmosphere. In this scenario, a reduction in the acid concentration may also become practicable by arresting or slowing the chain with the help of suitable radical scavengers. A scavenger, however, is expected to show markedly different reactivity toward the two chain carriers ($SO_5^{\bullet-}$ and $SO_4^{\bullet-}$). The $SO_5^{\bullet-}$ radical has a moderate oxidizing power[7] but can also participate in O-atom and H-atom transfer reactions. On the other hand, $SO_4^{\bullet-}$ radical is a strong oxidant and is also capable of oxidizing chemicals by H-atom abstraction.[8] Therefore, to have a realistic control over any atmospheric scenario, not only all the reaction kinetics pertaining to Scheme 1 but also the appropriate radical-scavenging abilities of any potential additive must be known precisely.

A search for $SO_x^{\bullet-}$ radical ($x = 3, 4, 5$) reactivity in the solution kinetic database[9] reveals that the magnitudes of the concerned $SO_3^{\bullet-}$ and $SO_4^{\bullet-}$ radical rate constants from different studies agree fairly well with each other. On the other hand, as shown in Table 1, despite many laboratory studies in pristine aqueous matrix, the six $SO_5^{\bullet-}$ reaction rates disagree considerably with each other. Although these disagreements probably reflect the differences in individual measurement procedures, a resulting major concern is the repeated use of some of these values for modeling atmospheric sulfuric acid generation.[5,6] Without any satisfactory explanation or supporting evidence for their specific choice of a set of rate values, the atmospheric projections in these modeling studies still remain mainly speculative, and therefore, their charted acid concentration, chain length, or other related conclusions may be far removed from reality.

To surmount this prevailing uncertainty in an otherwise important aspect of atmospheric chemistry, in this study we first present a new experimental approach to obtain fresh estimations of these reaction rates. Subsequently, using our values, we quantify the chain oxidation, and therein measure the potency of any $SO_5^{\bullet-}$ radical scavenger in controlling the chain length and resulting sulfuric acid concentration. However, before we present our study, it is advantageous to know the reasons behind such a large spread in rate values in Table 1.

The previous measurements were made employing either of the following two complementary techniques. In the majority of these experiments, oxygenated solutions of HSO_3^-/SO_3^{2-} were used in pulse radiolytic (PR) measurements, while in laser flash photolytic (LFP) studies either oxygenated HSO_3^-/SO_3^{2-} or $S_2O_6^{2-}$ solution was used.[10−17] Keeping the nature and complexity of reactions in Scheme 1 in perspective (i.e., occurrence of both radical−radical and radical−solute reactions), we can visualize the inherently unhelpful nature of the HSO_3^-/SO_3^{2-} matrix where all six or at least four major $SO_5^{\bullet-}$ radical reactions are expected to take place at any instant. In LFP with $S_2O_6^{2-}$, reaction 8

$$SO_5^{\bullet-} + S_2O_6^{2-} \rightarrow SO_4^{\bullet-} + S_2O_7^{2-} \qquad (8)$$

probably took place along with reactions 2 and 5.

Although reaction 8 has not yet been quantified, no better explanation can be offered at this stage for the reported rapid formation of $SO_4^{\bullet-}$ radical following a first-order kinetics.[13]

The acid dissociation constants of S(IV) species in water at 25 °C (1.26×10^{-2} and 5×10^{-7} M respectively for H_2SO_3 and HSO_3^-)[18] suggest that near neutral pH or in acidic pH all four radical−solute reactions 3 and 4 are possible; therefore, their differently mixed propensities may also have been a source of mismatch between two results obtained at different pH values. Additionally, the simultaneous presence of all three $SO_x^{\bullet-}$ radicals (shown below in Figure 9) and their overlapping absorption characteristics[10] are expected to produce complex kinetic traces. Thus, reported first- or second-order rates were actually oversimplification of these. In short, wide scatter in the $SO_5^{\bullet-}$ radical rate constant values originated or persisted because (i) indirect methods overlooking unaccounted for radical loss were repeatedly used to generate it, (ii) radical−radical reactions could never be segregated or studied separately from the radical−solute reactions, and (iii) as a consequence, during kinetic fittings of experimental results, inappropriate or incomplete assumptions were made, sometimes disregarding the ionic strength effect.

During our recent PR study on sulfur oxyanion radicals,[7] we found that the alternative method for obtaining the $SO_5^{\bullet-}$ radical from oxidation of HSO_5^- is simple, direct, and effective if certain precautions are taken. The starting solute Oxone (from DuPont as triple salt $2KHSO_5 \cdot KHSO_4 \cdot K_2SO_4$) and its solutions require some special handling, and from the expertise gathered during the above study, we were successful in designing appropriate matrixes to study the radical−radical reactions first. After quantifying these two reactions, subsequently the other sets of radical−solute reactions were studied. With careful selection of experimental pH and control and correlation of ionic strength (I) in these studies, a consistent set of six rate constants was estimated that was able to provide satisfactory analysis of all measurements.

Experimental Section

Materials and Procedure. All solutions were prepared in NanoPure water. The gases O_2, N_2, and N_2O used for purging solutions were obtained locally from British Oxygen Ltd. (purity ≈99.95%). Inorganic chemicals Na_2SO_3, Na_2SO_4, $KHSO_4$, KOH, KCl, KH_2PO_4, Na_2HPO_4, Na_3PO_4, and $HClO_4$ were of the highest purity available from Merck or Sigma. The Oxone samples were obtained from two suppliers, Aldrich and Lan-

caster. The actual fractions of $KHSO_5$ in these samples were estimated separately from spectrophotometric estimation of liberated I_2 (as I_3^- at 352 nm; $\epsilon = 25\,800\ M^{-1}\ cm^{-1}$ at pH 7) generated by HSO_5^- reaction with excess I^-. In the Aldrich sample, the HSO_5^- concentration was found to be ~94−96% of the above molecular formula, while in the Lancaster sample the concentration was lower, ~75−77%. The only other anion in both these samples was found to be sulfate (HSO_4^-/SO_4^{2-}). These and other spectral measurements were made on a Hitachi 330 spectrophotometer. All measurements were made close to 25 °C.

The 7 MeV pulse radiolysis−kinetic spectrophotometric detection setup used in this study has been described in detail before.[19,20] Samples were irradiated in a 1 cm square Suprasil cell. Optical detection of transients was performed within the spectral range of 230−800 nm using a 450 W xenon lamp and a Kratos monochromator blazed at 300 nm coupled to a Hamamatsu R-955 photomultiplier tube. A spectral resolution of ≈3 nm was routinely achieved, and the effect of scattered light at 250 nm was <2%.

A solution of Oxone has a pH <3 mainly due to the presence of HSO_4^-/SO_4^{2-} ($pK_a = 1.92$).[18] In general, Oxone solution (i.e., the HSO_5^- fraction) is thermally unstable at high concentrations. The extent of its decomposition or thermal instability was first checked separately at different pH values. It was found that while a few mM HSO_5^- was stable (at least 98% of starting value) for a long time (1 h), at ≥100 mM concentration its decomposition was ~15% during the same time. In alkaline pH close to 10 (in the presence of added KOH), the decomposition rate was high; a 3 mM starting concentration reduced to ~500 μM in 1 h. To minimize any uncertainty in a measurement arising out of HSO_5^- decomposition, in most cases Oxone solutions were used within 15 min. Additionally, for studies in the alkaline pH, a matrix with the desired pH was generated directly in the irradiation cell using a premixer assembly coupled to the flow system (similar to the one discussed in our previous study).[7] In this case, Oxone solution (pH <3) flowing in one channel was mixed with required amounts of alkali (or with appropriate amounts of phosphate buffer) flowing in the other channel at the same rate. Sample flow time from the mixing zone to the irradiation cell was <2 s, and any thermal decomposition during this period even in alkaline pH was found negligible. The sample pH was also recorded at the exit of the sample cell.

Similar sample premixing was found necessary for studies with HSO_3^-/SO_3^{2-} when either O_2 or Oxone was also needed along with it. Details of these matrix designs are discussed below at appropriate places in the text. For a study set, when variable amounts of Oxone (or HSO_3^-/SO_3^{2-}) were used, it was found desirable to add a balance amount of an equimolar mixture of HSO_4^-/SO_4^{2-}. The balance amount was equal to the difference of maximum Oxone (or HSO_3^-/SO_3^{2-}) concentration used in the set and the working Oxone (or HSO_3^-/SO_3^{2-}) for each measurement. Thus, the total amounts of HSO_x^-/SO_x^{2-} ($x = 4$ and 5 for Oxone or $x = 3$ and 4 for HSO_3^-/SO_3^{2-}) remained almost the same in any set of measurements. Although it increased the ionic strength, it offered advantages such as (a) ease in pH adjustment, especially in comparative studies, and (b) the same concentration of SO_4^{2-} for $Cl^\bullet$ radical reactions, and it prevented changes in experimental conditions in a series of measurements. In both spectral and kinetic measurements several oscilloscope traces at each wavelength were averaged for improving the signal-to-noise ratio. For kinetic studies requiring high ionic strength, Na_2SO_4 was used.

Dosimetry was performed with an aerated 10 mM SCN^- solution, and $G\epsilon$ and $G(SCN)_2^{\bullet-}$ values were taken as $2.59 \times 10^{-4}\ m^2\ J^{-1}$ and $3.5 \times 10^{-7}\ mol\ J^{-1}$, respectively, at 475 nm.[21] The parameters measured in pulse radiolysis experiments generally have an uncertainty of ±10−15%, which applies to all subsequent results of this study.

Beyond the experiments, kinetic fitting of experimental data was done with the help of the ACUCHEM Complex Reaction Modeling Package developed at NIST.[22] To achieve this, the rate constants of all reactions, the prevailing concentrations of the reacting radicals or solutes, and their molar absorptivities at the experimental wavelength are required. Most of the rate constants were obtained from the literature; ones not available were first measured and a few were accepted from comparison of similar reactions reported in the literature (Appendix A). For kinetic analysis, the concentrations of reacting species were obtained from the amounts of solutes added in solution and from the dose- and pulse-dependent yields of species radiolytically generated from water (Appendix B). The aim was to overlay the experimental traces with the ACUCHEM produced kinetics in the best possible form. Only from such fittings could various mixed processes be resolved satisfactorily and the detailed picture of Scheme 1 emerge.

During the ACUCHEM analyses, if any reaction involving two ionic species was referred to from the literature, the concerned experimental ionic strength was also estimated from the available matrix details. Then for the sake of convenience, all such rate values were extrapolated and recorded for a condition representing $I \rightarrow 0$ using the Debye−Hückel relation. Only if the necessary experimental details were not available for any measurement was the reported value accepted without any change. Similarly, all rates measured in this study were also recorded for the $I \rightarrow 0$ condition. This approach helped in utilizing the results from one measurement into a subsequent one. For each ACUCHEM analysis the concerned rates at $I \rightarrow 0$ were appropriately modified depending on the specific experimental condition being analyzed.

Results and Discussion

Radiolysis of dilute aqueous solution generates both oxidizing ($^\bullet OH$, hydroxyl radical) and reducing radicals (H-atom and e_{aq}^-) from water.[23,24] At pH >3.5, if the solutions are saturated with N_2O, the e_{aq}^- is converted into $^\bullet OH$ radical, doubling its yield (first two reactions in Table 2). If an 1:1 mixture of N_2O and O_2 gas is used for purging, $HO_3^\bullet/O_3^{\bullet-}$ and $HO_2^\bullet/O_2^{\bullet-}$ radicals are also produced from $^\bullet O^-$ and $e_{aq}^-/H^\bullet$ reactions shown in Table 2. The rate constants for these radical reactions are taken from the literature.[9,23] These rate constants have been used in all ACUCHEM kinetic analyses with any modification (due to ionic strength) needed. In the range of pH 2.5−12 some solutes and radicals undergo deprotonation. The concerned reactions are also included in Table 2. It may be noted that some other reactions that have negligible propensity have not been included, either in Table 2 or below.

$SO_5^{\bullet-}$ Radical Absorption Characteristics. In neutral and acidic pH, the rate constant of $^\bullet OH$ reaction with HSO_5^- ($^-O_3SOOH$) in reaction 9

$$^\bullet OH + HSO_5^- \rightarrow SO_5^{\bullet-} + H_2O \qquad (9)$$

is reported to be low ($1.7 \times 10^7\ M^{-1}\ s^{-1}$).[25]

Therefore, a significant fraction of the $^\bullet OH$ radical is expected to be lost in other reactions unless high concentration of Oxone

TABLE 2: Rate Constants for Radiation-Induced Homogeneous Radical−Radical and Some Radical−Solute Reactions and Different Solute pK_a Values[a]

reactions	rate constant[b] (M^{-1} s^{-1})
$e_{aq}^- + N_2O \rightarrow {}^\bullet O^- + N_2$	9.1×10^9 (ref 23)
${}^\bullet O^- + H_2O \rightarrow {}^\bullet OH + OH^-$	9.4×10^7 (ref 48)
${}^\bullet OH + OH^- \rightarrow {}^\bullet O^- + H_2O$	1.3×10^{10} (ref 48)
${}^\bullet OH + {}^\bullet OH \rightarrow H_2O_2$	5.5×10^9 (ref 23)
${}^\bullet OH + H_2O_2 \rightarrow HO_2^\bullet + H_2O$	2.7×10^7 (ref 23)
${}^\bullet OH + H^\bullet \rightarrow H_2O$	7.0×10^9 (ref 49)
${}^\bullet OH + O_2^{\bullet-} \rightarrow O_2 + OH^-$	1.1×10^{10} (ref 50)
${}^\bullet OH + HO_2^\bullet \rightarrow H_2O + O_2$	1.0×10^{10} (ref 51)
$H^\bullet + H^\bullet \rightarrow H_2$	5.0×10^9 (ref 23)
$H^\bullet + O_2 \rightarrow HO_2^\bullet$	1.2×10^{10} (ref 23)
$H^\bullet + HO_2^\bullet \rightarrow H_2O_2$	2.0×10^{10} (ref 52)
$H^\bullet + N_2O \rightarrow N_2 + {}^\bullet OH$	2.1×10^6 (ref 53)
$e_{aq}^- + e_{aq}^- \rightarrow 2OH^-$	5.5×10^9 (ref 23)
$e_{aq}^- + O_2 \rightarrow O_2^{\bullet-}$	1.9×10^{10} (ref 23)
$e_{aq}^- + {}^\bullet OH \rightarrow OH^-$	3.3×10^{10} (ref 54)
$e_{aq}^- + H^\bullet \rightarrow OH^- + H_2$	2.5×10^{10} (ref 54)
$e_{aq}^- + H_2O_2 \rightarrow OH^- + {}^\bullet OH$	1.3×10^{10} (ref 54)
$e_{aq}^- + H_3O^+ \rightarrow H^\bullet + H_2O$	2.3×10^{10} (ref 23
$O_2^{\bullet-} + HO_2^\bullet \rightarrow H_2O_2 + O_2$	9.7×10^7 (ref 55)
${}^\bullet O^- + O_2 \rightarrow O_3^{\bullet-}$	2.0×10^9 (ref 23)
$O_3^{\bullet-} + H_2O \rightarrow HO_3^\bullet + OH^-$	8.5×10^9 (ref 34)

[a] pK_a: $HO_2^\bullet/O_2^{\bullet-}$ = 4.8 (ref 55); ${}^\bullet OH/{}^\bullet O^-$ = 11.9 (ref 48); $HO_3^\bullet/O_3^{\bullet-}$ = 8.2 (ref 34); HSO_5^-/SO_5^{2-} = 9.4 (ref 56); HSO_3^-/SO_3^{2-} = 7.2 (ref 18); HSO_4^-/SO_4^{2-} = 1.92 (ref 18); H_2O_2/HO_2^- = 11.7 (ref 23). [b] In refs 23 and 55 values are selected/recommended.

can be used. However, restricted then by HSO_5^- thermal instability, the alternative choice of reaction 10

$$ {}^\bullet OH + SO_5^{2-} \rightarrow SO_5^{\bullet-} + OH^- \qquad (10) $$

in alkaline pH ($k = 2.1 \times 10^9$ M^{-1} s^{-1})[25] was appropriate for a quantitative generation of the $SO_5^{\bullet-}$ radical. Employing a dose of 104 Gy to an N_2O saturated 2.5 mM Oxone (Aldrich) solution at pH 11.5, the $SO_5^{\bullet-}$ radical was produced with $G(SO_5^{\bullet-}) \sim 0.57$ μmol J^{-1}. The flow mixer assembly was used with N_2O saturated Oxone solution in one channel and N_2O saturated solution of appropriate amount of KOH in the other channel. The resulting after-pulse $SO_5^{\bullet-}$ radical absorption spectrum is shown in Figure 1. The parent SO_5^{2-} absorption spectrum is included in Figure 1 to account for its bleaching. A molar absorptivity value of 1065 M^{-1} cm^{-1} for the $SO_5^{\bullet-}$ radical is obtained at the 260−265 nm peak after taking into account the loss of parent SO_5^{2-} absorption. Although most of the previous studies on the $SO_5^{\bullet-}$ radical absorption spectrum generally agreed on the spectral profile and its λ_{peak} value at 260−265 nm, there was considerable disagreement on the reported ϵ value (ranging from ~700 to 1030 M^{-1} cm^{-1}).[10,13,16,26] In those studies, the $SO_5^{\bullet-}$ radical was generated via the $SO_3^{\bullet-}$ radical. Under those conditions loss (small but unaccounted fraction) of the parent $SO_3^{\bullet-}$ radical due to its dimerization reaction and loss of $SO_5^{\bullet-}$ radical following radical−solute reactions (large fraction) are expected. At present, if rates from Table 1 are used, the loss due to the latter reactions might seem negligible; however, as shown later in this study, these are significant. Thus, the actual yield of the $SO_5^{\bullet-}$ radical was always less than the assumed value and this difference was reflected in the lower measure of ϵ value reported in all cases. The only study using impure Caro's acid[12] reported direct generation of $SO_5^{\bullet-}$ radical and an ϵ value of ~1000 M^{-1} cm^{-1} at ~260 nm. In our experiment, the clean matrix also ensured that such impurity effects or unaccounted for radical loss remained minimal, resulting in the best possible representation of the $SO_5^{\bullet-}$ radical absorption characteristics.

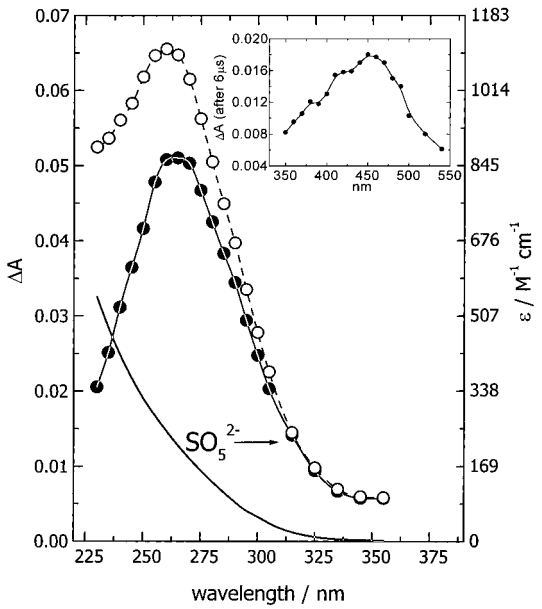

Figure 1. $SO_5^{\bullet-}$ radical absorption spectrum at pH 11.5 (−●−). Equal volume of N_2O saturated 5.0 mM HSO_5^- solution mixed with N_2O saturated KOH; dose = 104 Gy; $G(SO_5^{\bullet-})$ taken = 0.57 μmol J^{-1} for calculation of ϵ. Transient spectrum corrected for SO_5^{2-} bleaching (−○−) from its absorption (—). Inset: Transient absorption spectrum obtained 6 μs after the end of pulse.

In Figure 1 (inset), the transient absorption spectrum above 300 nm obtained 6 μs after the end of pulse is shown. This spectral profile matches well with the $SO_4^{\bullet-}$ radical absorption spectrum[10,27] and is expected to form following only reaction 2. From experimental ΔA_{max} values at 440−450 nm and the absorbed dose, the maximum yield of the $SO_4^{\bullet-}$ radical is found to be ~20% of the $SO_5^{\bullet-}$ radical yield in the experimental matrix. The remaining $SO_5^{\bullet-}$ radicals are expected to react following only reaction 5. As shown in Table 1, the branching ratio of reactions 2 and 5 in previous studies reveal a wide scatter, with values ranging from ~0.04 to 0.9.[9−17] In our measurement, it is to be noted that, unlike the inactive product $S_2O_8^{2-}$ formed by reaction 5, the $SO_4^{\bullet-}$ radical from reaction 2 is reactive toward matrix components such as SO_5^{2-} and OH^-. Thus, the $SO_4^{\bullet-}$ radical absorbance maximum cannot be a true measure of its maximum yield. In this case, even the concentration of $S_2O_8^{2-}$ as an end product, and consequently the branching of reaction 5, cannot be correlated with the initial radical yield as $S_2O_8^{2-}$ also forms following reaction 7. Therefore, a true picture of the branching ratio cannot be obtained from mere experimental measure of $\Delta A_{445\,nm}$ or final $S_2O_8^{2-}$ concentration. Instead, only detailed kinetic analyses of experimental traces are expected to provide the ratio k_2/k_5. Details of such ACUCHEM analyses are presented below. However, some other related and constitutive measurements for use in such studies are first presented in the next section.

HSO_5^- Reaction with H-atom. In N_2 saturated solutions below pH 4, with increasing acidity, it was observed that the after-pulse yield of the $SO_4^{\bullet-}$ radical increased rapidly. The rate constant for H-atom reaction with H_2SO_5 generating the $SO_4^{\bullet-}$ radical is reported to be ca. 1.3×10^8 M^{-1} s^{-1}.[28] However, in acidic pH the two reported e_{aq}^- scavenging reactions by H_3O^+ and HSO_5^- also need to be taken into account with the latter producing 80% ${}^\bullet OH$ radical and 20% $SO_4^{\bullet-}$ radical.[26] Experimentally, in pH ~2.5 Oxone solution (Lancaster sample, 1.5 mM) where only ~ 2% of HSO_5^- remains as H_2SO_5 (first pK_a of Caro's acid ~1), the observed after-pulse yield of $SO_4^{\bullet-}$ radical could not be explained only on the basis of H_2SO_5/e_{aq}^-

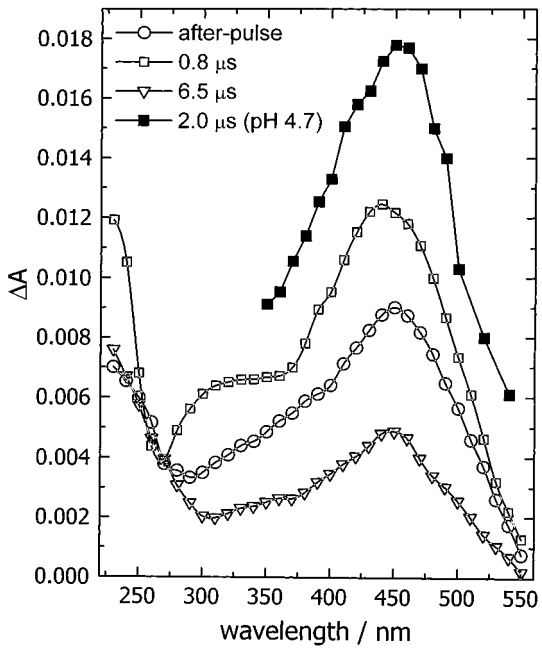

Figure 2. Time-resolved transient spectra in pH 2.5, N_2 saturated 20 mM HSO_5^- solution with 0.2 M *tert*-butyl alcohol; dose = 35 Gy; $G(SO_4^{\bullet-}) \sim 0.21$ μmol J^{-1}. Transient spectrum at pH 4.7 in the presence of 1.2 M $H_2PO_4^-$, 20 mM HSO_5^-, and 0.05 M *tert*-butyl alcohol is also included for comparison; dose = 92 Gy; $G(SO_4^{\bullet-}) \sim 0.12$ μmol J^{-1}.

reactions. Therefore, to check if an additional reaction

$$H^{\bullet} + HSO_5^- \rightarrow H_2O + SO_4^{\bullet-} \qquad (11)$$

was responsible for the observed $SO_4^{\bullet-}$ radical generation, first a spectral measurement was made employing a dose of 35 Gy with N_2 saturated 14 mM Oxone solution at pH ~2.5 containing 0.2 M *tert*-butyl alcohol.

The time-resolved transient spectra shown in Figure 2 indicates that the $SO_4^{\bullet-}$ radical yield is ~0.21 μmol J^{-1}. The value is close to $G(H^{\bullet})$ {$=g(H^{\bullet}) + [g(e_{aq}^-)]f$ (where f = fraction of e_{aq}^- reacting with H_3O^+) + $G(SO_4^{\bullet-})$ from 20% of the remaining $e_{aq}^- + HSO_5^-$ reaction}, suggesting the existence of reaction 11. The increase in transient absorption below 300 nm in Figure 2 is due to the β-hydroxy radical produced from reaction of $^{\bullet}$OH with *tert*-butyl alcohol.[29] Employing 50 ns pulses delivering 14 Gy dose to N_2 saturated solutions containing 0.1 M *tert*-butyl alcohol and 0.5−3.0 mM Oxone (Lancaster) at pH 2.5 (with balance HSO_4^-/SO_4^{2-}), the reaction 11 kinetics was measured. The kinetic traces (not shown here) at 450 nm in this case showed a two-step formation of the $SO_4^{\bullet-}$ radical. In the first step it was rapidly generated from the $e_{aq}^- + HSO_5^-$ reaction (with ~20% branching as before), and in the slower step it was obtained from reaction 11. An overall rate value ca. $(8.5 \pm 0.7) \times 10^7$ M^{-1} s^{-1} was obtained for $SO_4^{\bullet-}$ radical formation rate in the slower step. Taking into account the rate constant of H-atom reaction with H_2SO_5 and its contribution at pH 2.5, k_{11} was estimated to be ca. $(8.0 \pm 0.7) \times 10^7$ M^{-1} s^{-1}. Similar spectral and kinetic measurements at pH ~4.7 also supported these results. These studies were possible in the presence of ~1.0 M $H_2PO_4^-$ following the method proposed by Ye et al.[30] In this set of measurements with N_2 saturated solutions of 50 mM *tert*-butyl alcohol and 0.5−2.5 mM Oxone, k_{11} was estimated tobe ca. $(8.7 \pm 1.2) \times 10^7$ M^{-1} s^{-1}. The e_{aq}^- was again partially converted to H-atom as a result of its reaction with $H_2PO_4^-$.

The transient spectrum obtained for 92 Gy dose in the presence of 1.2 M $H_2PO_4^-$, 50 mM *tert*-butyl alcohol, and 14 mM Oxone is also included in Figure 2 for comparison. In this matrix the total $G(SO_4^{\bullet-})$ is seen to be ~0.12 μmol J^{-1} {$=g(H^{\bullet}) + [g(e_{aq}^-)]f$ (where f = fraction of e_{aq}^- reacting with H_3O^+) + $G(SO_4^{\bullet-})$ from 20% of remaining $e_{aq}^- + HSO_5^-$ reaction}. In these measurements, made at a pH more than 3 units away from the first pK_a of H_2SO_5, any interference from it is expected to be negligible. Additionally, interference from $H_2PO_4^{\bullet}$ radical produced in the $^{\bullet}OH + H_2PO_4^-$ reaction is also expected to be negligible in the microsecond time scale of measurement.[31] In these measurements, however, in the presence of such a high concentration of salt, the $SO_4^{\bullet-}$ radical decay reactions become faster and the resulting k_{11} values have a larger uncertainty than our previous estimate at pH 2.5. The above sets of results have no direct relation to the main aim of our study, but since at pH ≥4 $G(H^{\bullet})$ remains ~65 nmol J^{-1},[23] they nevertheless allowed us quantification of H-atom reactions in the presence of Oxone. Thus, the general practice of ignoring the same in oxidative PR studies was avoided.

Reaction Kinetics of the $SO_4^{\bullet-}$ Radical with HSO_5^-/SO_5^{2-}. During the course of our main study, we frequently encountered situations where the $SO_4^{\bullet-}$ radical formed in the presence of solutes HSO_5^-/SO_5^{2-}. Then oxidation of HSO_5^-/SO_5^{2-} respectively by H-atom or electron transfer reactions 12 and 13 is expected.

$$SO_4^{\bullet-} + HSO_5^- \rightarrow SO_5^{\bullet-} + HSO_4^- \qquad (12)$$

$$SO_4^{\bullet-} + SO_5^{2-} \rightarrow SO_5^{\bullet-} + SO_4^{2-} \qquad (13)$$

Only one limiting estimate of reaction 12 kinetics is available from the literature ($k_{12} < 1.0 \times 10^5$ M^{-1} s^{-1}),[25] but no estimate is available for k_{13}. The magnitude of k_{12} was first verified employing a matrix consisting of N_2 saturated acidic solution of Oxone. To minimize reaction complexity, no $^{\bullet}$OH scavenger was used. Low propensity of reaction 9 then allowed only partial generation of $SO_5^{\bullet-}$ radical and a large fraction of $^{\bullet}$OH decayed following other reactions of Tables 2 and 3. The $SO_4^{\bullet-}$ radical formed by reaction 11 or otherwise from reaction 2 decayed mainly following radical dimerization reaction 7, following reaction 12, and following its radical−radical reaction with the remaining $^{\bullet}$OH.[32] (Its minor reactions include reactions with the remaining H-atom, $HO_2^{\bullet}$ radical, H_2O_2, and H_2O.) The decay trace at 450 nm shown in Figure 3 was obtained employing a dose of 34 Gy in a N_2 saturated solution at pH 2.8 containing 5 mM Oxone (Aldrich), 10 mM each K_2SO_4 and $KHSO_4$ at I ca. 80 mM. The value of k_7 in this matrix was taken ca. 1.0×10^9 M^{-1} s^{-1}. The presence of some $SO_5^{\bullet-}$ radical necessitated use of accurate k_2 and k_5 values in ACUCHEM analysis, and these were obtained from results discussed in the next section (see Appendix C). The best ACUCHEM overlay was obtained for $k_{12} = (1.6 \pm 0.2) \times 10^6$ M^{-1} s^{-1}. To change experimental conditions, the dose (between 20 and 40 Gy using 520 ns pulse), the Oxone concentration (2−8 mM with balance HSO_4^-/SO_4^{2-}), and the working pH (between 2 and 3.5) were varied separately. From ACUCHEM analysis of these results an average $k_{12} = (1.0 \pm 0.1) \times 10^6$ M^{-1} s^{-1} was obtained for $I \rightarrow 0$. Figure 3 also compares the ACUCHEM analysis if the previously reported literature value of $\sim 1.0 \times 10^5$ M^{-1} s^{-1} or some other k_{12} value (at $I \rightarrow 0$) is used. From the nature of these kinetic overlays, we conclude that our rate value satisfying a wider range of experimental conditions and incorporating analyses of all major and minor reactions provides the best description for

TABLE 3: Generation and Reactions of $SO_4^{\bullet-}$ Radical in N_2 Saturated Solution of HSO_5^- or $S_2O_8^{2-}$ and Formation and Reactions of $SO_3^{\bullet-}$ Radical

reactions	rate constant (M^{-1} s^{-1})
$e_{aq}^- + S_2O_8^{2-} \rightarrow SO_4^{\bullet-} + SO_4^{2-}$	1.2×10^{10} (ref 23)[a]
$e_{aq}^- + HSO_5^- \rightarrow {}^{\bullet}OH + SO_4^{2-}$	8.4×10^9 (ref 26)
$e_{aq}^- + HSO_5^- \rightarrow OH^- + SO_4^{\bullet-}$	2.1×10^9 (ref 26)
$H^{\bullet} + S_2O_8^{2-} \rightarrow HSO_4^- + SO_4^{\bullet-}$	1.4×10^7 (ref 28)
$H^{\bullet} + H_2SO_5 \rightarrow SO_4^{\bullet-} + H_3O^+$	1.3×10^8 (ref 28)
$H^{\bullet} + HSO_5^- \rightarrow SO_4^{\bullet-} + H_2O$	8.0×10^7 (this study)
${}^{\bullet}OH + S_2O_8^{2-} \rightarrow S_2O_8^{\bullet-} + OH^-$	1.2×10^7 (ref 57)
${}^{\bullet}OH + HSO_5^- \rightarrow SO_5^{\bullet-} + H_2O$	5.0×10^6 (this study)
${}^{\bullet}OH + SO_5^{2-} \rightarrow SO_5^{\bullet-} + OH^-$	2.1×10^9 (ref 25)
${}^{\bullet}OH + SO_4^{\bullet-} \rightarrow HSO_5^-$	1.0×10^{10} (ref 32)
$SO_5^{\bullet-} + HO_2^{\bullet} \rightarrow HSO_5^- + O_2$	5.0×10^7 (ref 58)
$SO_5^{\bullet-} + SO_5^{\bullet-} \rightarrow S_2O_8^{2-} + O_2$	2.2×10^8 (this study)
$SO_5^{\bullet-} + SO_5^{\bullet-} \rightarrow 2SO_4^{\bullet-} + O_2$	2.1×10^8 (this study)
$SO_4^{\bullet-} + SO_4^{\bullet-} \rightarrow S_2O_8^{2-}$	7.0×10^8 (see Appendix A)
$SO_4^{\bullet-} + HSO_5^- \rightarrow HSO_4^- + SO_5^{\bullet-}$	1.0×10^6 (this study)
$SO_4^{\bullet-} + SO_5^{2-} \rightarrow SO_4^{2-} + SO_5^{\bullet-}$	1.0×10^8 (this study)
$SO_4^{\bullet-} + S_2O_8^{2-} \rightarrow SO_4^{2-} + S_2O_8^{\bullet-}$	6.3×10^5 (ref 16)
$SO_4^{\bullet-} + OH^- \rightarrow SO_4^{2-} + {}^{\bullet}OH$	2.0×10^7 (ref 9; for $I \rightarrow 0$)
$SO_4^{\bullet-} + H_2O \rightarrow HSO_4^- + {}^{\bullet}OH$	9.3 (ref 16)
$SO_4^{\bullet-} + HO_2^{\bullet} \rightarrow HSO_4^- + O_2$	3.5×10^9 (ref 59)
$SO_4^{\bullet-} + O_2^{\bullet-} \rightarrow SO_4^{2-} + O_2$	6.0×10^9 (assumed)
$SO_4^{\bullet-} + H_2O_2 \rightarrow HO_2^{\bullet} + SO_4^{2-} + H_3O^+$	1.2×10^7 (ref 31)
${}^{\bullet}OH + HSO_3^- \rightarrow SO_3^{\bullet-} + H_2O$	4.5×10^9 (ref 11)
${}^{\bullet}OH + SO_3^{2-} \rightarrow SO_3^{\bullet-} + OH^-$	5.4×10^9 (ref 11)
$SO_3^{\bullet-} + SO_3^{\bullet-} \rightarrow S_2O_6^{2-}$	2.4×10^8 (ref 9; for $I \rightarrow 0$)
$SO_3^{\bullet-} + SO_3^{\bullet-} \rightarrow SO_3^{2-} + SO_3$	3.2×10^8 (ref 9; for $I \rightarrow 0$)
$SO_3^{\bullet-} + O_2 \rightarrow SO_5^{\bullet-}$	1.1×10^9 (see Appendix A)

[a] In ref 23 values are selected/recommended.

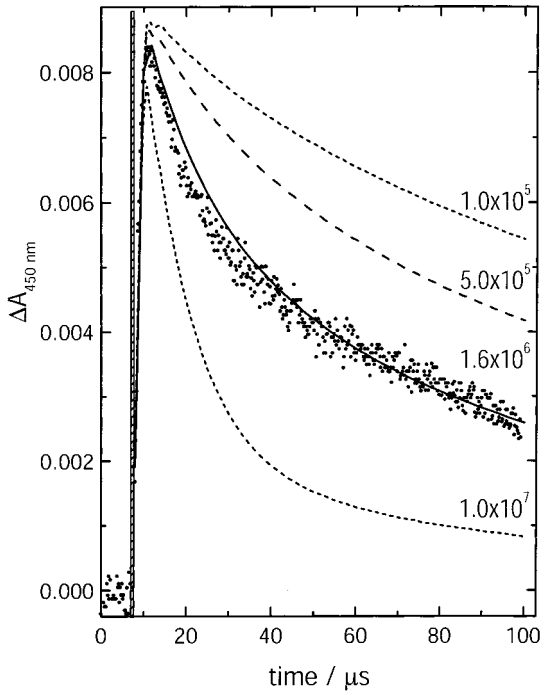

Figure 3. Decay trace at 450 nm obtained employing dose of 34 Gy in a N_2 saturated solution at pH 2.8 containing 10 mM HSO_5^- and 10 mM each of K_2SO_4 and $KHSO_4$ (I ca. 0.08 M). Lines (— and ---) represent ACUCHEM kinetic analysis with different k_{12} values for $I \rightarrow 0$. See text for explanation. See Appendix B for an explanation of shaded area shown in this and other figures.

reaction 12 kinetics. In the previous study a similar detailed analysis is not reported.

To measure k_{13}, experiments were carried out in mildly alkaline pH. In a typical experiment, a dose of 15 Gy was used. In the flow mixer assembly, in one channel N_2 saturated Oxone solution (amounts varied from 0.25 to 2.0 mM) along with balance HSO_4^-/SO_4^{2-} was used while the other channel carried 2 mM N_2 saturated $S_2O_8^{2-}$ solution with appropriate amounts of KOH. The final matrix pH in these experiments was maintained within ±0.1 unit of the target value 10 by using a calculated amount of KOH proportional to the prevailing HSO_4^- and HSO_5^- concentrations in solution. The pH was also checked at the cell exit before radiolysis. Unlike in acidic pH, ${}^{\bullet}OH$ was efficiently scavenged by the SO_5^{2-} anion. As a consequence, in addition to the direct formation of $SO_4^{\bullet-}$ radical following the first reaction of Table 3, it was also continuously regenerated by reaction 2. Taking into consideration appropriate reactions from Table 3 for alkaline pH, and following a similar approach as described for acidic solutions, the best-fit value of k_{13} at the experimental $I \sim 30$ mM was $(2.0 \pm 0.3) \times 10^8$ M^{-1} s^{-1}. The k_{13} value reduces to ca. $(1.0 \pm 0.2) \times 10^8$ M^{-1} s^{-1} at $I \rightarrow 0$.

$SO_5^{\bullet-}$ Radical Decay Kinetics and Yield of the $SO_4^{\bullet-}$ Radical. The radical−radical reactions 2 and 5 could not be isolated in past studies. Therefore, our evaluation of reactions in Scheme 1 started with these reactions so that accurate evaluation of the radical−solute reactions was subsequently possible. The most convenient way to measure $SO_5^{\bullet-}$ radical decay was by following the simultaneous formation of reaction 2 product, i.e., the $SO_4^{\bullet-}$ radical. The working solution pH was restricted between 3.5 and 11 since $SO_4^{\bullet-}$ radical kinetics above pH 12 was severely affected due to its rapid reaction with OH^- (Table 3). For the sake of convenience, initially measurements were made at fixed solution pH 4, 7.9, and 10.4. Taking a cue from our earlier $SO_5^{\bullet-}$ radical spectral results, a high dose of 115 Gy (2.2 μs fwhm pulse) was used to overcome a low yield of $SO_4^{\bullet-}$ radical. To keep the reaction complexities to a minimum, buffer was avoided in these measurements. An N_2O saturated 1.4 mM Oxone solution (Lancaster sample) was used in all cases. At the three selected solution pH values, prevailing starting concentrations of the solutes (mM) $H_2SO_5/HSO_5^-/SO_5^{2-}/HSO_4^-/SO_4^{2-}$ were: $0.002/2.158/77 \times 10^{-5}/0.027/3.2$ respectively at pH 4, ∼0/2.094/0.066/∼0/3.23 at pH 7.9, and ∼0/0.196/1.96/∼0/3.23 at pH 10.4. The $SO_4^{\bullet-}$ radical kinetic traces were recorded at 450 nm while the decay traces originating mainly from parent $SO_5^{\bullet-}$ radical were recorded at 260 nm. Next, ACUCHEM analysis of each trace was performed. At 260 nm, apart from the $SO_5^{\bullet-}$ radical, other species that show appreciable/significant absorbance are $SO_4^{\bullet-}$ radical ($\epsilon = 400$ M^{-1} cm^{-1}), ${}^{\bullet}OH$ (475), H_2O_2 (12), $S_2O_8^{2-}$ (14), $O_2^{\bullet-}$ radical (1680), and $HO_2^{\bullet}$ radical (520).[27] To account for the loss of parent (HSO_5^-/SO_5^{2-}) absorption at different pH values, the apparent ϵ for the $SO_5^{\bullet-}$ radical in these analyses was taken as follows: 875 M^{-1} cm^{-1} at pH 10.4, 980 at pH 7.9, and 1025 at pH 4. At 450 nm, the $SO_4^{\bullet-}$ radical is the only species that showed significant absorption and its $\epsilon_{450\ nm}$ value was taken as 1630 M^{-1} cm^{-1}.[10] For kinetic analysis, apart from the $SO_5^{\bullet-}$ radical−radical decay reactions 2 and 5, other pertinent reactions from Tables 2 and 3 including reactions of different species arising out of water radiolysis, $SO_5^{\bullet-}$ radical generation by ${}^{\bullet}OH$ reaction (also see the last paragraph of this section), $SO_4^{\bullet-}$ radical generation by the H-atom, and $SO_4^{\bullet-}$ radical reactions with ${}^{\bullet}OH$, H_2O, OH^-, HSO_5^-/SO_5^{2-}, etc. were taken into consideration.

Figure 4 shows the 260 nm $SO_5^{\bullet-}$ radical decay (mixed with some $SO_4^{\bullet-}$ radical formation/decay, especially at later stages) and 450 nm (only) $SO_4^{\bullet-}$ radical formation/decay traces. Appropriate ACUCHEM analyses are also shown superimposed on the respective experimental traces. These kinetic overlays at the experimental $I = 12-16$ mM were possible with a uniform pair of values of $(2.9 \pm 0.4) \times 10^8$ and $(2.8 \pm 0.4) \times$

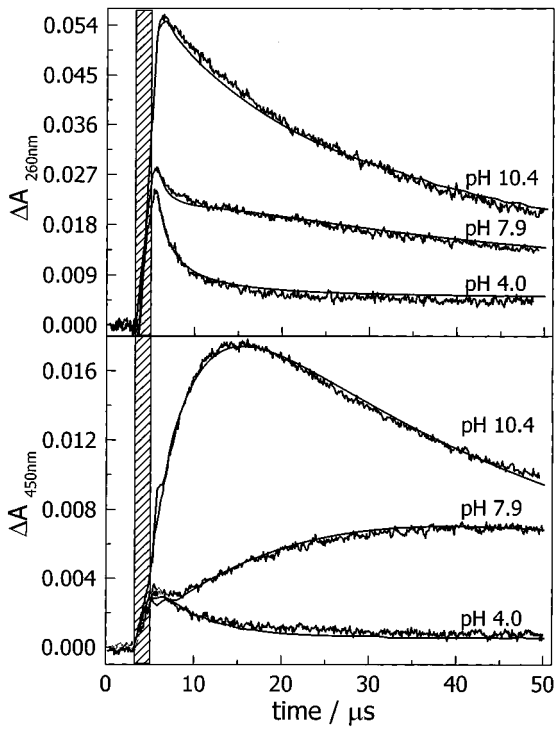

Figure 4. Kinetic traces for $SO_5^{\bullet-}$ radical−radical reactions. Dose = 115 Gy in 2.2 mM N_2O saturated HSO_5^- solution. Lines (—) represent ACUCHEM kinetic analysis with k_2 and k_5 values reported in the text for $I \rightarrow 0$.

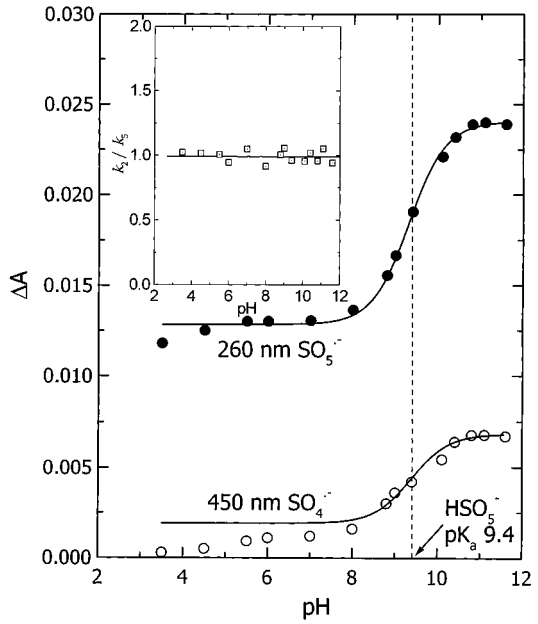

Figure 5. After-pulse ΔA_{max} at 260 nm (parent bleach corrected, $SO_5^{\bullet-}$ radical) and 450 nm ($SO_4^{\bullet-}$ radical) obtained at different solution pH values. Inset: Branching ratio (k_2/k_5) obtained from ACUCHEM analysis of kinetic traces covering the experimental pH range.

10^8 M^{-1} s^{-1}, respectively, for k_2 and k_5. At $I \rightarrow 0$ the respective values reduce to ca. $(2.2 \pm 0.3) \times 10^8$ and $(2.1 \pm 0.3) \times 10^8$ M^{-1} s^{-1}, indicating almost equal propensity of reactions 2 and 5. These measurements were subsequently made at other pH values covering the working range, and the results are shown in Figure 5. The observed maximum after-pulse absorbances at 260 nm (mainly due to the $SO_5^{\bullet-}$ radical) and 450 nm ($SO_4^{\bullet-}$ radical) are plotted against the pH value. The yields of $SO_5^{\bullet-}$ (and consequently the $SO_4^{\bullet-}$ radical) followed the HSO_5^- pK_a (9.4, Table 2) because of relative values of k_9 and k_{10}. ACUCHEM analysis of kinetic traces gave satisfactory overlays with k_2 and k_5 values of similar magnitude as obtained above. Therefore, as shown in Figure 5 (inset), the branching ratio (k_2/k_5) over the pH range remained ∼1. Even when some of these measurements were repeated at high ionic strength in the presence of Na_2SO_4 (∼0.4 M), no significant deviations were noticed in the results if all concerned ionic reaction rates were first modified accordingly. These results indicate that reactions 2 and 5 probably take place independent of each other.

Our k_2 and k_5 values differ significantly from the previous suggestions shown in Table 1, in respect to both their magnitudes and their branching ratio. A comparison is strictly not possible due to entirely different approaches taken earlier. For example, referring to some values in Table 1, the frequently referred sets in the literature were reported by Huie and Neta[11] ($k_2 = 6.0 \times 10^8$ and $k_5 = 1.4 \times 10^8$ M^{-1} s^{-1}) and were later used for modeling by Deister and Warneck,[14] Rudich et al.,[5] van den Berg et al.,[6] and others. Other values were suggested by Buxton et al.[10] (k_2/k_5 ca. $2.2 \times 10^8/4.8 \times 10^7$ M^{-1} s^{-1}, respectively), Herrman et al.[16] (k_2/k_5 ca. $5.2 \times 10^6/1.2 \times 10^8$ M^{-1} s^{-1}, respectively), and Yermakov et al.[15] (k_2/k_5 ca. $8.7 \times 10^7/1.4 \times 10^7$ M^{-1} s^{-1}, respectively). The actual effects of radical−solute reactions on these indirect results are presented in the next section, where the effects of S(IV) on $SO_5^{\bullet-}$ radical decay is revealed. With [S(IV)] > [$SO_5^{\bullet-}$], these reactions always modified the product $SO_4^{\bullet-}$ radical yield and formation kinetics. However, in analysis of radical kinetics, these concerned reactions were not granted due importance, and as a result these estimations were severely affected.

In the above studies, when kinetic traces obtained in acidic and near neutral pH were subjected to ACUCHEM analysis, use of the k_9 value reported by Maruthamuthu and Neta[25] produced higher yields and faster formation kinetics for $SO_5^{\bullet-}$ radical as compared to the corresponding experimental traces. Even in the presence of a few tens of mM Oxone concentration, the measured experimental yields of the $SO_5^{\bullet-}$ radical and its formation rates remained less than half of the calculated values based on the above rate. To arrive at a consensus k_9 value, a fresh estimation of $G(SO_5^{\bullet-})$ was made using a reactivity formula similar to the proposal of Schuler et al.[33] The experimental $SO_5^{\bullet-}$ radical concentrations obtained at high Oxone concentrations were compared with their projected values, and the two sets matched closely only if the previous k_9 value (=1.7×10^7 M^{-1} s^{-1}) was reduced by ∼70% to ca. $(5.0 \pm 0.3) \times 10^6$ M^{-1} s^{-1}. The results obtained are shown in Table 4. For such high concentrations of Oxone, any thermal loss of HSO_5^- during the time interval of each measurement (∼4−8%) was measured separately and the correction factor taken into consideration. To measure the kinetics, a dose of 15 Gy was used. To calculate $SO_5^{\bullet-}$ radical concentration from the 260 nm trace, contributions of reaction 11 and $\epsilon_{260\,nm}$ of the $SO_4^{\bullet-}$ radical (400 $M^{-1}cm^{-1}$) as well as absorption from $^{\bullet}OH$ and $HO_2^{\bullet}$ radicals and the bleaching of the parent HSO_5^- absorption ($\epsilon = 40$ M^{-1} cm^{-1}, making effective $\epsilon(SO_5^{\bullet-})_{260\,nm} = 1025$ M^{-1} cm^{-1}) were also taken into account. In this context, if a comparison is made for H-atom abstraction reactions from H_2O_2 and $HO_2^{\bullet}$ radical by $^{\bullet}OH/SO_4^{\bullet-}$ radicals, it is observed that the respective oxidation rates are within 1 order of magnitude from each other.[9] The rate constants of H-atom abstraction from HSO_5^- having a similar −OOH group are also expected to remain close to each other, and our lower k_9 and higher k_{12} values are further supported by this trend. Thus, this

TABLE 4: Yield of $SO_5^{\bullet-}$ Radical in N_2O Saturated Solution at pH ≈ 5 in the Presence of High Concentration of HSO_5^-

$[HSO_5^-]$ (M)	I^a (M)	$\Delta A_{260\ nm}$(max)	$[SO_4^{\bullet-}]^b$ (μM)	$[SO_5^{\bullet-}]$ (μM) obsd	$[SO_5^{\bullet-}]^c$ (μM) $k = 5.0 \times 10^6\ M^{-1}\ s^{-1}$	$[SO_5^{\bullet-}]^c$ (μM) $k = 1.7 \times 10^7\ M^{-1}\ s^{-1}$
0.05	0.2	0.008 27 ± 0.000 28	1.53	7.41	7.43	7.57
0.1	0.4	0.008 36 ± 0.000 22	1.64	7.47	7.50	7.64
0.2	0.8	0.008 41 ± 0.000 25	1.68	7.54	7.55	7.72
0.3	1.2	0.008 50 ± 0.000 19	1.71	7.62	7.64	7.80

[a] I decides the fraction of ($e_{aq}^- + HSO_5^-$) wrt the total ($e_{aq}^- + HSO_5^-$) + ($e_{aq}^- + N_2O$). [b] $G(SO_4^{\bullet-}) = g(H^\bullet) + g(e_{aq}^-)$\{0.2[fraction of ($e_{aq}^- + HSO_5^-$)]\}. [c] $G(SO_5^{\bullet-}) = g(^\bullet OH) + g(e_{aq}^-)$\{0.8[fraction of ($e_{aq}^- + HSO_5^-$) + fraction of ($e_{aq}^- + N_2O$)]\}.

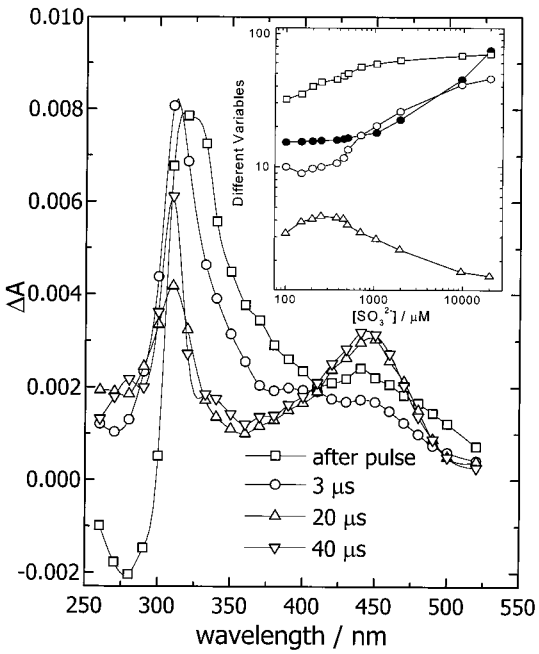

Figure 6. Time-resolved transient spectra obtained in 75 μM SO_3^{2-} and 5 mM HPO_4^{2-} pH 9 solution with 110 Gy dose. Solution saturated with N_2O and O_2 in 1:1 ratio. Inset: Effect of progressive increase in SO_3^{2-} concentration on various parameters: (−□−) $[SO_3^{\bullet-}]$; (−●−) ionic strength; (−○−) $[SO_3^{\bullet-}]/[SO_4^{\bullet-}]$; (−△−) $[SO_4^{\bullet-}]$.

lower k_9 value was used in all the ACUCHEM analyses mentioned earlier and also later in the text.

$SO_5^{\bullet-}$ Reactions with HSO_3^-/SO_3^{2-}. A comparison of the one-electron reduction potentials of $SO_5^{\bullet-}$ and $SO_3^{\bullet-}$ radicals ($\Delta E = 0.08$ V [7]) suggest that in the case of equilibrium reaction 14 in alkaline pH, the equilibrium constant K (i.e., k_f/k_b) value would be low, ∼23.[8]

$$SO_5^{\bullet-} + SO_3^{2-} \leftrightarrow SO_5^{2-} + SO_3^{\bullet-} \qquad (14)$$

Since the O-atom transfer reaction 3 is expected to compete with equilibrium 14, experimental measurement of either k_f or k_b may not be possible directly. Indeed, separate attempts to measure these rate constants (keeping [solute]/[radical] ratio > 25 in either case) failed, and only $SO_4^{\bullet-}$ radical formation could be confirmed, suggesting a higher propensity of reaction 3 as compared to reaction 4.

As an example, the time-resolved spectra obtained in a solution of 75 μM SO_3^{2-} under irradiation with 110 Gy dose is shown in Figure 6. The N_2O saturated SO_3^{2-} solutions at pH 9 (with 5 mM buffer) flowing in one channel was mixed with equal proportion to O_2 saturated buffer solution at pH 9 in the other channel. For such a low SO_3^{2-} concentration, the majority of $SO_4^{\bullet-}$ radical was presumably formed by reaction 2. The observed A_{max} (450 nm) value indicates ∼10% $SO_4^{\bullet-}$ radical yield compared to the after-pulse $SO_3^{\bullet-}$ radical concentration. However, when the SO_3^{2-} concentration was progressively increased, as shown in Figure 6 (inset), the resulting $SO_4^{\bullet-}$ radical concentration first showed an increase (up to a few 100 μM SO_3^{2-} concentration) and thereafter decreased steadily with further increase in SO_3^{2-} concentration (from 0.4 to 20 mM). Although the $SO_3^{\bullet-}$ radical yield increased continuously as a result of increase in reactivity in its generation (the $SO_5^{\bullet-}$ radical yield is expected to follow the $SO_3^{\bullet-}$ radical in the presence of O_2), the observed faster rate of increase in concentration of $SO_4^{\bullet-}$ radical as compared to the $SO_3^{\bullet-}$ radical (for first few 100 μM SO_3^{2-} concentration) suggests that, in addition to reaction 2, the $SO_4^{\bullet-}$ radical also formed following reaction 3 at higher solute concentration. On the other hand, the observed reduction in $SO_4^{\bullet-}$ radical yield in the case of SO_3^{2-} concentration >0.4 mM resulted from its enhanced scavenging by SO_3^{2-}. These qualitative observations predict comparative or close magnitudes of k_2, k_4, and possibly k_3; i.e., the latter values are expected to be $>10^7\ M^{-1}\ s^{-1}$. Table 1 reveals only a few k_3 and k_4 values meeting this order while most of the others are significantly low. To arrive at consensus k_3 and k_4 values, a reevaluation of reactions 3 and 4 was made as follows.

The PR study by Buxton et al.[10] with a few mM SO_3^{2-} concentration reports ∼7% yield of $SO_4^{\bullet-}$ radical with respect to the initial yield of the oxidizing radical. A similar conclusion is drawn from the plot in Figure 6 (inset). In other words, a high dose producing an initial high concentration of the oxidizing radical ($^\bullet OH$ in this case) is necessary for obtaining even moderate $SO_4^{\bullet-}$ radical absorption signals. The HSO_3^- pK_a of 7.2 and HSO_5^- pK_a of 9.4 also necessitated two separate working pH ranges of 4−4.5 and 9.5−11.5.

In alkaline pH, the $SO_5^{\bullet-}$ radical could be generated following either of the following two methods. In the first method, it was obtained from oxidation of N_2O saturated solution of Oxone. In this case, N_2O saturated few mM Oxone solutions (Aldrich sample, balanced with Na_2SO_4) were mixed in equal proportions with N_2O saturated solution containing an appropriate amount of S(IV). The required amount of alkali or buffer for achieving the desired experimental pH was used in the S(IV) channel. The ratio of $[SO_5^{2-}]/[SO_3^{2-}]$ (the latter in the 0.1−0.4 mM range and balanced with Na_2SO_4) was maintained ≥25 so that mainly the $SO_5^{\bullet-}$ radical was generated from $^\bullet OH$. In the second method, N_2O saturated S(IV) solution was mixed in 1:1 volume ratio with O_2 saturated alkali/buffer solution producing 12.5 mM N_2O and 0.64 mM O_2 concentrations in the irradiation cell. In this case SO_3^{2-} concentration could be varied over the 0.1−5 mM range (balanced with Na_2SO_4) and the yield of $SO_3^{\bullet-}$ radical and subsequently the $SO_5^{\bullet-}$ radical were taken to be ∼0.52 μmol J^{-1}.[10] In either case, for a few selected solute concentrations, subsequently the dose was also increased from ∼50 to 120 Gy to increase the influence of reactions 2 and 5. For ACUCHEM analysis of the resulting kinetic traces, appropriate reactions from Tables 2 and 3 were considered (after taking into account the solution I in each case) and only the rates k_3 and k_4 (representing $SO_5^{\bullet-} + SO_3^{2-}$ reactions) were systematically varied, covering the range of 10^6−$10^9\ M^{-1}\ s^{-1}$.

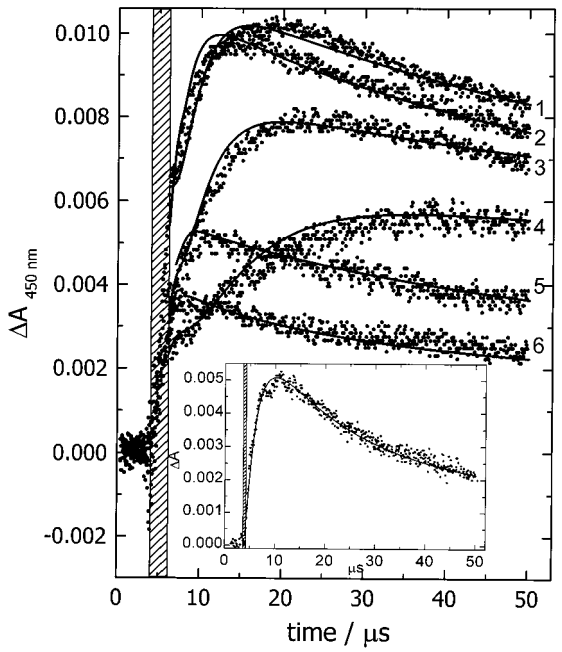

Figure 7. Kinetic traces and ACUCHEM overlay for measurements in alkaline pH range 10−10.6. pH adjusted with KOH; dose = 102 Gy with 2.2 μs pulse. Traces for N_2O/O_2 saturated SO_3^{2-} solutions: (4) 100 μM; (3) 300 μM; (1) 400 μM; (2) 750 μM; (5) 1.95 mM; (6) 4.8 mM. Inset: Experimental trace and ACUCHEM overlay for N_2O saturated pH 10.5 solution of 2.5 mM SO_5^{2-} and 100 μM SO_3^{2-}; dose = 48 Gy with 520 ns pulse.

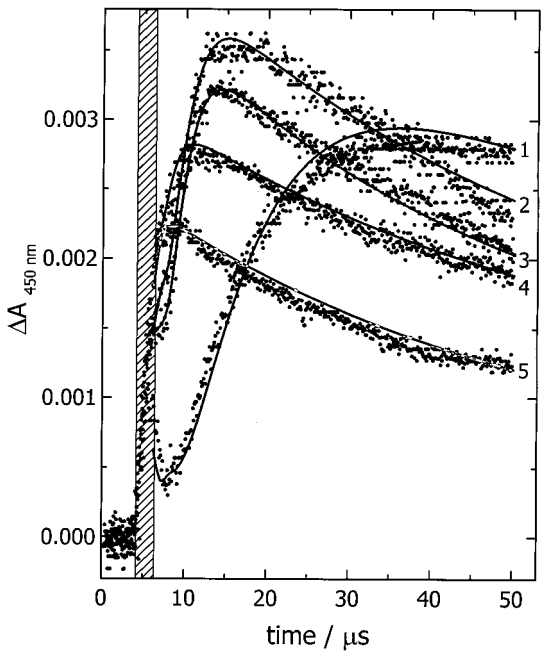

Figure 8. Kinetic traces and ACUCHEM overlay for measurements in acidic pH range 3.8−4.5. pH adjusted with $HClO_4$; dose = 102 Gy with 2.2 μs pulse. Traces for N_2O/O_2 saturated HSO_3^- solutions: (1) 135 μM; (2) 650 μM; (4) 1.95 mM; (5) 4.8 mM. Trace 3 with 6 mM $H_2PO_4^-$ (no $HClO_4$) for 650 μM HSO_3^-.

The k_2 and k_5 values from the previous section were used to account for the $SO_5^{\bullet-}$ radical−radical reactions. At 450 nm, apart from the $SO_3^{\bullet-}$ and $SO_4^{\bullet-}$ radicals, only the $O_3^{\bullet-}$ radical has significant absorption ($\epsilon_{450\,nm} = 1700\ M^{-1}\ cm^{-1}$).[27,34] The best kinetic analyses of the traces and correlation of the $SO_4^{\bullet-}$ radical yields obtained by the first method (at $I = 60-100$ mM) were possible with k_3 values within $(1.3-1.8) \times 10^9\ M^{-1}\ s^{-1}$ and k_4 values within $(2.4-3.3) \times 10^8\ M^{-1}\ s^{-1}$. In the second method (at $I = 10-30$ mM) the respective k_3 and k_4 values remained within $(9.2-12.0) \times 10^8\ M^{-1}\ s^{-1}$ and $(1.6-2.2) \times 10^8\ M^{-1}\ s^{-1}$. Taking into account results from all other related measurements, at $I \rightarrow 0$ the k_3 and k_4 values reduce to ca. $(5.6 \pm 0.6) \times 10^8$ and $(1.0 \pm 0.1) \times 10^8\ M^{-1}\ s^{-1}$.

Some experimental traces with ACUCHEM analyzed overlays are shown in Figure 7. The relative magnitudes of k_3 and k_4 values indicate that only ∼15% of the $SO_5^{\bullet-} + SO_3^{2-}$ reaction follow the electron transfer path and a majority (∼85%) lead to the formation of $SO_4^{\bullet-}$ radical by O-atom transfer. The higher propensity of the O-atom transfer reaction explains our earlier unsuccessful attempt to follow the equilibrium (14) kinetics.

In acidic pH, the rate of reaction 9 is almost 3 orders of magnitude less than the corresponding rate ($4.5 \times 10^9\ M^{-1}\ s^{-1}$) of $^{\bullet}OH + HSO_3^-$ reaction 15.[11]

$$HSO_3^- + {}^{\bullet}OH \rightarrow SO_3^{\bullet-} + H_2O \qquad (15)$$

Therefore, unlike in alkaline pH, to preferentially generate $SO_5^{\bullet-}$ radical from HSO_5^- following the first method would necessitate use of very high concentrations (>100 mM) of Oxone. Due to thermal instability of such a high concentration of HSO_5^- in solution and also due to its reported thermal reaction with HSO_3^-,[35] only the second method could be used. Similar to the alkaline pH measurements, in this case HSO_3^- solution with (1:1) N_2O and O_2 saturation was used. In acidic pH, at 450 nm only the $SO_3^{\bullet-}$ and $SO_4^{\bullet-}$ radicals show absorption while the $HO_3^{\bullet}$ radical pK_a (=8.2 and $\epsilon_{450\,nm} < 10\ M^{-1}\ cm^{-1}$) ensures complete protonation of any $O_3^{\bullet-}$ radical formed.[34] Thus, no contribution from $O_3^{\bullet-}$ radical is expected in these cases. Employing the previously estimated k_2 and k_5 values (and also k_3 and k_4 values to account for any SO_3^{2-} present even in acidic pH), satisfactory analyses of experimental traces representing the HSO_3^- reactions were possible with the following set of rate values. In the case of $I \sim 0.4$ mM, the k_3 and k_4 values ranged over $(5.9-6.7) \times 10^7$ and $(2.8-3.4) \times 10^7\ M^{-1}\ s^{-1}$, respectively. At $I \sim 11$ mM representing higher concentration of solutes, the respective k_3 and k_4 values marginally increased to $(7.0-8.0) \times 10^7$ and $(3.4-4.1) \times 10^7\ M^{-1}\ s^{-1}$. Taking into account the ionic strengths in different cases, at $I \rightarrow 0$, the k_3 and k_4 values (for HSO_3^-) reduce to ca. $(6.0 \pm 0.4) \times 10^7$ and $(3.0 \pm 0.3) \times 10^7\ M^{-1}\ s^{-1}$, respectively.

A few experimental traces and their respective ACUCHEM analyses are shown in Figure 8. A comparison of these traces reveals that, at low solute concentration, the after-pulse maximum absorbance first decreased and then increased before its final slower decay (to the baseline value). In alkaline pH with only SO_3^{2-}, the effect, however, was less pronounced (Figure 7). The time-resolved absorption spectra shown in Figure 6 clearly reveal that the first after-pulse maximum is mainly due to the $SO_3^{\bullet-}$ radical, as expected from reactions 9 and 15, and that the second maximum is due to the $SO_4^{\bullet-}$ radical. The intervening $SO_5^{\bullet-}$ radical, however, does not absorb at 450 nm. When the solutions were saturated only with N_2O, the second maximum vanished completely. In that case, formation of neither $SO_5^{\bullet-}$ nor $SO_4^{\bullet-}$ radical took place, supporting our after-pulse peak assignment even in the presence of O_2.

Buxton et al.[10] have claimed that, in the presence of dissolved O_2, the after-pulse (i.e., first) maximum arises mainly from the $O_3^{\bullet-}$ radical produced from O_2 addition to $^{\bullet}O^-$ radical formed as a result of e_{aq}^- scavenging by N_2O (see reactions in Table 2). In our analysis it was observed that even in alkaline pH in the presence of SO_3^{2-}, as in their experiments, the prevailing concentration of $O_3^{\bullet-}$ radical accounts for only a part of the

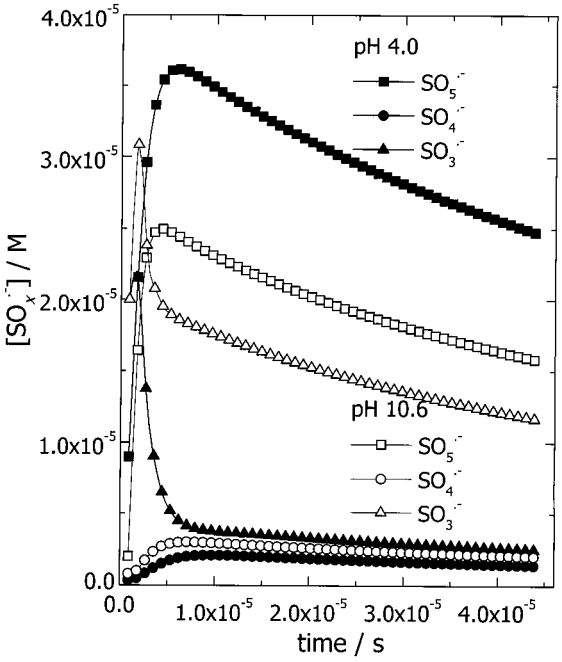

Figure 9. ACUCHEM analysis of two representative traces from Figures 7 and 8 showing simultaneous presence of all three $SO_x^{\bullet-}$ radicals. Acid pH $[HSO_3^-] = 650$ μM; Alkaline pH $[SO_3^{2-}] = 750$ μM.

observed after-pulse transient absorbance. For example, in the presence of 100 μM SO_3^{2-} at pH 10.5, the ACUCHEM projected after-pulse concentration of $O_3^{\bullet-} + HO_3^{\bullet}$ radicals is $\sim 10^{-6}$ M and has only $\sim$60% contribution toward the transient absorption. However, in acidic pH these values are almost negligible. In addition, the $O_3^{\bullet-}$ radical shows a broad absorption profile with λ_{max} close to 430 nm while the $HO_3^{\bullet}$ radical absorption is less intense ($\lambda_{max} = 350$, $\epsilon_{350\,nm} = 300$ M^{-1} cm^{-1}).[34] Both are quite different from the after-pulse absorption profile with λ_{max} at 260 nm shown in Figure 6. Additionally, at the experimental pH 9 in their study, the reaction scheme dealing with reported protonation of $O_3^{\bullet-}$ radical is not supported by the pK_a value of 8.2 for $HO_3^{\bullet}/O_3^{\bullet-}$ reported by Büehler et al.[34] Therefore, the set of reactions used in data analysis in the paper by Buxton et al.[10] seems to be incomplete. Similar omissions or overlook of many prevalent (but maybe unknown then) reactions in other studies explains the wide scatter in Table 1 rate values. The final support of our mechanism comes from the quality of ACUCHEM analysis of the experimental traces shown in Figures 7 and 8. Earlier, Buxton et al.[10] failed to achieve a complete fitting of any experimental trace with their scheme stressing $O_3^{\bullet-}/HO_3^{\bullet}$ reactions.

In earlier sections we have hinted that oxygenated S(IV) matrix used in some previous studies was an inappropriate selection for estimating k_2 and k_5. Figure 9 clearly shows that, in the presence of O_2 and even a few 100 μM S(IV), all three $SO_x^{\bullet-}$ radicals coexist after initiation of oxidation and proves the following. (i) Interference due to $SO_4^{\bullet-}$ radical absorption is significant even during the estimation of $SO_3^{\bullet-} + O_2 \rightarrow SO_5^{\bullet-}$ reaction kinetics[10,11] (also see Appendix A). (ii) Unless [$SO_5^{\bullet-}$ radical] $\gg$ [S(IV)], all radical−solute reactions 3 and 4 contribute significantly and alter the desired effects of reactions 2 and 5, apparently increasing $SO_4^{\bullet-}$ radical generation. Thus, these two types of reactions needed to be separately quantified, and it has been accomplished only in this study.

Reactions in the Presence of Cl^-. In the above experiments, even a high initial radical concentration produced only a moderate concentration of $SO_4^{\bullet-}$ radical and consequently modest absorption signals. To boost the signal strength, two approaches were possible: (i) use of a higher absorbed dose and (ii) suitable modification of the reaction scheme to generate a radical with high molar absorptivity. In our experimental setup the first possibility could not be adopted because of the upper limitation on available dose of $\sim$125 Gy from the accelerator. (Even otherwise, beyond a limiting high dose, to offset the resulting increases in radical−radical reactions, high solute concentrations would be necessary. At high solute and O_2 concentrations, associated thermal changes are expected to increase the level of uncertainty in results. Limited solubility of O_2 in water may also prevent ideal matrix design beyond a few 100 Gy dose.) The second approach was instead practicable with the use of Cl^- and with a moderate dose of 36 Gy from a 500 ns pulse. In presence of $SO_4^{\bullet-}$ radical, Cl^- quantitatively produces $Cl_2^{\bullet-}$ radical that shows more intense absorption ($\epsilon_{345\,nm} = 8800$ M^{-1} cm^{-1})[27] than the $SO_4^{\bullet-}$ radical. To further examine the degree of consistency in our rate measurements, a few studies were repeated in N_2O/O_2 saturated acidic (buffered) matrix with HSO_3^- and Cl^-. For kinetic analysis of these traces, along with reactions from Tables 2 and 3, additional reactions from Table 5 were required to account for the $Cl_2^{\bullet-}$ radical generation and reactions.[9,36−41]

TABLE 5: Reaction Scheme in the Presence of Cl^-

reactions	rate constant (M^{-1} s^{-1})
$SO_4^{\bullet-} + Cl^- \rightarrow Cl^{\bullet} + SO_4^{2-}$	3.0×10^8 (ref 9; for $I \rightarrow 0$)
$Cl^{\bullet} + SO_4^{2-} \rightarrow Cl^- + SO_4^{\bullet-}$	2.5×10^8 (ref 37)
$Cl^- + {}^{\bullet}OH \rightarrow ClOH^{\bullet-}$	4.3×10^9 (ref 36)
$ClOH^{\bullet-} \rightarrow Cl^- + {}^{\bullet}OH$	6.1×10^9 (ref 36)
$Cl^{\bullet} + OH^- \rightarrow ClOH^{\bullet-}$	$1.^8 \times 10^{10}$ (ref 38)
$ClOH^{\bullet-} + H_3O^+ \rightarrow Cl^{\bullet} + H_2O$	2.1×10^{10} (assumed)
$Cl^{\bullet} + H_2O \rightarrow ClOH^{\bullet-} + H_3O^+$	4.5×10^3 (ref 60)
$ClOH^{\bullet-} + Cl^- \rightarrow Cl_2^{\bullet-} + OH^-$	1.0×10^4 (ref 61; for $I \rightarrow 0$)
$Cl^{\bullet} + Cl^- \rightarrow Cl_2^{\bullet-}$	8.0×10^9 (ref 62)
$Cl_2^{\bullet-} \rightarrow Cl^{\bullet} + Cl^-$	1.1×10^5 (ref 36)
$Cl^{\bullet} + Cl^{\bullet} \rightarrow Cl_2$	1.0×10^8 (ref 39)
$Cl_2^{\bullet-} + O_2^{\bullet-} \rightarrow 2Cl^- + O_2$	1.0×10^9 (ref 9; for $I \rightarrow 0$)
$Cl_2^{\bullet-} + HO_2^{\bullet} \rightarrow 2Cl^- + O_2 + H_3O^+$	1.0×10^9 (ref 63)
$Cl_2^{\bullet-} + Cl_2^{\bullet-} \rightarrow Cl^- + Cl_3^-$	1.3×10^9 (ref 64)
$Cl_2^{\bullet-} + OH^- \rightarrow ClOH^{\bullet-} + Cl^-$	2.0×10^7 (ref 61; for $I \rightarrow 0$)
$Cl^{\bullet} + HSO_3^- \rightarrow Cl^- + SO_3^{\bullet-} + H_3O^+$	1.0×10^9 (assumed, comparing with related $Cl^{\bullet}$ reactions)
$Cl_2^{\bullet-} + HSO_3^- \rightarrow 2Cl^- + SO_3^{\bullet-} + H_3O^+$	1.8×10^8 (ref 9; for $I \rightarrow 0$)
$Cl_2^{\bullet-} + SO_3^{2-} \rightarrow 2Cl^- + SO_3^{\bullet-}$	5.0×10^8 (assumed, comparing with other $Cl_2^{\bullet-}$ reactions)
$Cl_2^{\bullet-} + HSO_5^- \rightarrow 2Cl^- + SO_5^{\bullet-} + H_3O^+$	$<1.0 \times 10^5$ (assumed, comparing with $SO_4^{\bullet-} + HSO_5^-$ reaction)
$Cl_2^{\bullet-} + SO_5^{2-} \rightarrow 2Cl^- + SO_5^{\bullet-}$	1.0×10^8 (assumed, comparing with $SO_4^{\bullet-} + SO_5^{2-}$ reaction)

Figure 10 shows some experimental kinetic traces and their ACUCHEM analysis. In this case, the volume ratio $N_2O:O_2$ was maintained ca. 3:2, producing 15 mM N_2O and 0.5 mM O_2 in the sample. Satisfactory overlay of experimental traces employing our set of k_2-k_5 values once again confirms their correct magnitude. These results also indicate that any missing reaction or reaction deliberately not included in these fitting exercises has negligible contribution. In the presence of Cl^- with only N_2O saturation, reactions of $O_2/O_2^{\bullet-}$, etc. were absent, but other reactions such as those of $ClOH^{\bullet-}$, $Cl^{\bullet}$, and $Cl_2^{\bullet-}$ radicals were existent. Thus, only a direct after-pulse formation of $Cl_2^{\bullet-}$ radical took place at pH 4.3. In the presence of O_2, when 20 mM phosphate (as NaH_2PO_4) was used at the same pH 4.3, the 345 nm trace showed a slightly faster kinetics mainly because of overall increase in the ionic reaction rates.

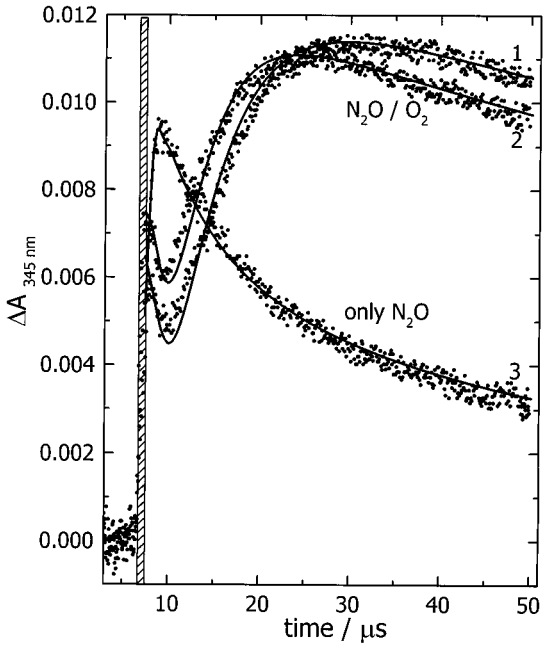

Figure 10. Kinetic traces and ACUCHEM overlay for measurements in acidic pH in the presence of 12 mM Cl^-. Dose = 38 Gy with 520 ns pulse. Traces for 3:2 N_2O/O_2 saturated 450 μM HSO_3^- solutions: (1) pH 3:9 adjusted with $HClO_4$; (2) pH 4.3 adjusted with 20 mM $H_2PO_4^-$; (3) N_2O saturated pH 4.3 solution with 20 mM $H_2PO_4^-$.

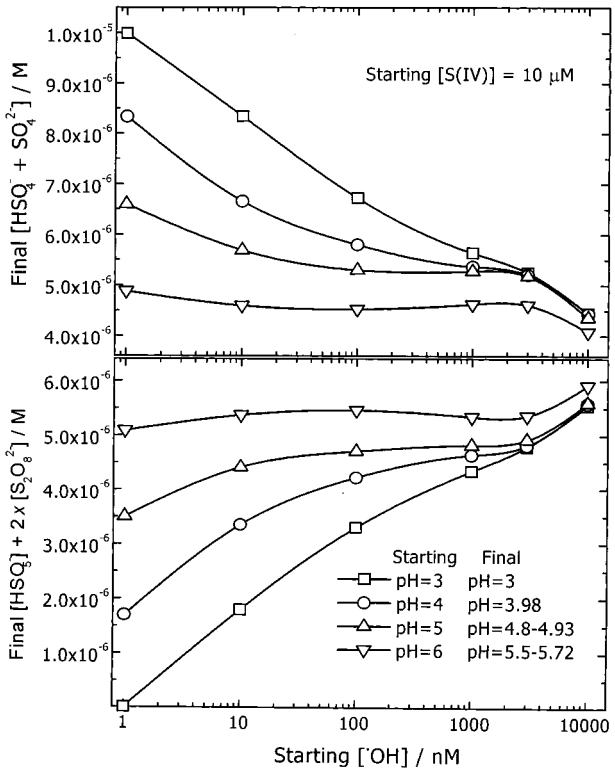

Figure 11. Simulation studies for chain oxidation of S(IV) in acidic solutions projecting concentrations of oxidized species under different conditions. Starting fixed concentration of S(IV) = 10 μM; O_2 = 240 μM. Conditions varied: pH from 3 to 6; initiating [$^\bullet$OH] from 1 nM to 10 μM. Final concentrations also include thermal reaction between HSO_5^- and HSO_3^-.

If any set of the lower estimate of k_3 and k_4 values from previous studies (Table 1) were reasonable, then even in the presence of high S(IV) concentrations (10−100 mM) the propensities of reactions 2 and 5 would not be expected to be significantly influenced. Consequently, chain lengths would fall much short of the projected value of 1000.[1] Employing our rate values instead, all such projections could be explained satisfactorily and these studies are presented below.

Chain Oxidation of S(IV) Revisited. First, taking into account reactions 1−7, chain oxidation was simulated in oxygenated HSO_3^- solutions, and next, possibilities of reducing sulfuric acid (mainly as HSO_4^-/SO_4^{2-}) production vis-à-vis atmospheric S(IV) oxidation were explored. In these simulation studies the second pK_a of HSO_3^-, HSO_4^-, and HSO_5^-, etc. (Table 2) were taken into account to correlate the resulting changes in matrix pH. The starting solute concentrations were taken as follows: O_2 = 240 μM (as present in an aerated solution) and total HSO_3^-/SO_3^{2-} = 10 μM (as expected in polluted atmosphere).[42] For the sake of convenience, $^\bullet$OH radical was taken as the chain initiator and its concentration was varied in different sets from 1 nM to 10 μM. The starting solution pH was separately changed from 3 to 6 in unit steps, reflecting different atmospheric scenarios.[43] After the chain oxidation, the possibility of thermal reaction between HSO_5^- formed and any remaining HSO_3^- was also included in these studies.[35]

The final results from these simulations are shown in Figure 11. Since, during the chain oxidation, the O_2 concentration remained ≫ radical concentration, almost complete conversion of $SO_3^{\bullet-}$ to $SO_5^{\bullet-}$ radical took place. This is supported by an almost negligible final concentration of $S_2O_6^{2-}$ anion obtained in all cases (not shown in Figure 11). Even for the highest starting $^\bullet$OH radical concentration used, the maximum product [$S_2O_6^{2-}$] was ∼1 nM. At low starting $^\bullet$OH radical concentration, the ratio [total sulfuric acid]/[$^\bullet$OH] was found to be as high as 10^4 and the concentration of other sulfur−oxygen species produced remained $<10^{-10}$ M. With increase in starting radical concentration, as the chain length decreased progressively and reached a value <10 for a few μM $^\bullet$OH radical concentration, the productions of other sulfur−oxygen species such as HSO_5^- and $S_2O_8^{2-}$ increased steadily from ∼pM level to ∼μM level. This trend of continuous reduction of chain length mainly resulted from the increasing propensities of radical−radical reactions that competed favorably with the radical−solute reactions even in the beginning stages. (As mentioned above, similar reduction in chain length was also observed even at low initiating radical concentration if any of the previous lower estimates of k_3 and k_4 from Table 1 were used.)

For a given value of the starting $^\bullet$OH radical concentration, the final sulfuric acid yield is greater in lower pH. Since we have already observed that the $SO_5^{\bullet-}$ radical dimerization rate constants are invariant over this selected pH range, this behavior may seem to contradict our other rate estimations wherein we found that all (chain) favoring radical−solute reactions involving the S(IV) species have lower propensity for HSO_3^- as compared to SO_3^{2-}. However, this slower change took place not because of the $SO_5^{\bullet-}$ radical reactions but only because of the strongly pH dependent thermal reaction 16.[35]

$$HSO_5^- + HSO_3^- \rightarrow 2HSO_4^- \qquad (16)$$

With decreasing pH, its rapidly increasing rate value (k = 1.04 + [H_3O^+] × 10^7 M^{-1} s^{-1}) ensured a simultaneous scavenging of any HSO_5^- formed and a corresponding increase in sulfuric acid concentration. This explanation was supported by a similar reaction scheme wherein reaction 16 was omitted. In this case the yield of sulfuric acid increased marginally from 4.6 to 4.7 μM going from pH 3 to pH 6 for 1 nM starting $^\bullet$OH radical concentration. At 10 μM starting $^\bullet$OH radical concentration, the corresponding values were 4.0−4.3 μM for pH 3 and pH 6,

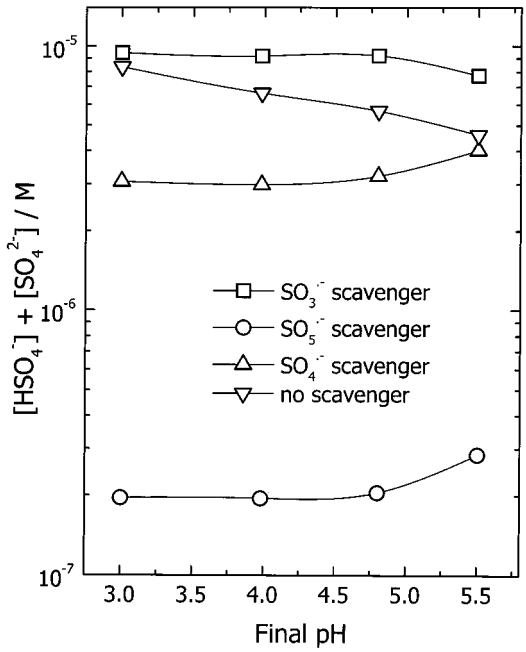

Figure 12. Scavenging of $SO_x^{\bullet-}$ radicals (x = 3, 4, 5) and related final concentration of sulfuric acid, inclusive of reaction 16. Assumed: [scavenger] = 1 μM; k(scavenging) = 10^8 M^{-1} s^{-1}; [$^{\bullet}$OH] = 10 nM; [S(IV)] = 10 μM; [O_2] = 240 μM.

respectively. In may be noted that in this set of studies we have ignored the possibility of photolysis of $S_2O_8^{2-}$ to the $SO_4^{\bullet-}$ radical, feasible in the presence of sunlight. If the photolysis rate competes with the rates of reaction 5 and 7, then the yield of sulfuric acid will increase further; however other trends would remain similar to the above results.

Continuing with the simulation studies, our next aim was to separately check the effects of scavenging the three $SO_x^{\bullet-}$ radicals, with the intent to reduce sulfuric acid concentrations. Radical scavenging is possible at every stage of the reactions, including the scavenging of the starting $^{\bullet}$OH radicals. However, the latter reactions are not considered here and only scavenging of the $SO_x^{\bullet-}$ radicals are discussed. At starting $^{\bullet}$OH radical concentration of 10 nM, total S(IV) concentration of 10 μM, and dissolved O_2 concentration of 240 μM, the extent of radical scavenging was separately considered for each $SO_x^{\bullet-}$ radical. To simplify the scheme, the starting scavenger concentration was taken as 1 μM and k_{17} was taken as 1×10^8 M^{-1} s^{-1}.

$$\text{scavenger} + SO_x^{\bullet-}\ (x = 3, 4, \text{or } 5) \rightarrow [\text{scavenger}]_{\text{oxidized}} + SO_x^{2-} \quad (17)$$

Figure 12 shows the effect of scavengers on the final sulfuric acid concentration including the effect of reaction 16. As above, reaction 16 once again played an important role in limiting the sulfuric acid concentration. The apparent higher value for acid concentration in the case of $SO_3^{\bullet-}$ radical scavenger as compared to the case when no scavenger was considered is due to reaction 16. On the other hand, when reaction 16 was not considered for a realistic evaluation of the role of scavengers in chain oxidation, the following results were obtained.

In the case of $SO_3^{\bullet-}$ radical scavenging, the high propensity of its reaction with O_2 was found to mask the effect of scavenger to a large extent and [sulfuric acid]$_{\text{final}}$ over the pH 3−6 reduced marginally from ∼4.4 μM in the absence of scavenger to 3.6−3.4 μM in the presence of scavenger. In this case, peroxymonosulfate anion (HSO_5^-) was the other major product. Its final concentrations were close to 4.8−5.5 μM for pH 3 and pH 6, respectively, in the absence of scavenger, and it decreases to 3.6−4.4 μM for pH 3 and pH 6, respectively, in the presence of the scavenger. About 30% and 20% S(IV) remains nonoxidized in the presence of scavenger at pH 3 and pH 6, respectively.

In the case of $SO_4^{\bullet-}$ radical scavenging, effect of scavenging was stronger. For example, both sulfuric acid and HSO_5^- concentrations remained ∼1 μM over pH 3−6. Thus, the efficiency of oxidative change decreased to ∼20−25% as compared to the absence of scavenger and ∼80% of S(IV) remains nonoxidized. If reaction 16 was taken into account, as expected, an additional 10% S(IV) (equivalent of the HSO_5^- yield) was thermally oxidized to give a final sulfuric acid concentration ca. 3 μM. However, when scavenging was considered for the $SO_5^{\bullet-}$ radical, the effects were found to be substantial. Over the pH range of interest, only ∼1% of S(IV) was oxidized and even with contribution from reaction 16 the value increased marginally to ∼2%. These results clearly indicate that, to break the chain oxidation and minimize sulfuric acid production, it is sufficient to utilize a suitable $SO_5^{\bullet-}$ radical scavenger with its reactivity (=concentration × scavenging rate) of ∼100 s^{-1}.

In the NIST database,[9] only a few aqueous medium reactions of the $SO_5^{\bullet-}$ radical are yet reported, and a majority of these involve electron transfer from a reducing species. However, since O-atom and H-atom transfer reactions are also possible, unless comprehensive kinetic results are available, possibilities of $SO_5^{\bullet-}$ radical scavenging by chemicals of atmospheric abundance will remain mainly speculative. However, even from these limited references we find that aromatic amines and $HO_2^{\bullet}$ radical show sufficient reactivity toward the $SO_5^{\bullet-}$ radical and presumably can act as scavengers under favorable conditions. In Bäckström's studies,[1] it was reported that diphenylamine inhibited the chain oxidation. The rate constant of reaction 18 is reported to be ca. 5×10^7 M^{-1} s^{-1}, [44] and its ability to influence the chain is explained from our above results.

$$SO_5^{\bullet-} + (C_6H_5)_2NH \rightarrow HSO_5^- + (C_6H_5)_2N^{\bullet} \quad (18)$$

On the other hand, reference to alcohols as chain retardants[1] or production of phenol in the presence of added benzene[45] can be explained by the reactions of $SO_4^{\bullet-}$ radical (and intermediate $^{\bullet}$OH radical from $SO_4^{\bullet-}$), the other chain carrier. Thus, satisfactory explanation of all the previous experimental results is available from our analysis of Scheme 1 reactions.

In Table 6 the six rate constants obtained in this study are presented for easy reference. It may be noted that the uncertainty in the rate value for $SO_5^{\bullet-} + HSO_3^- \rightarrow HSO_4^- + SO_4^{\bullet-}$ reaction is slightly lower than the generally accepted value of ±10−15% in PR measurements. On the other hand, the corresponding uncertainty for the reaction $SO_4^{\bullet-} + SO_5^{2-} \rightarrow SO_5^{\bullet-} + SO_4^{2-}$ is higher than the generally accepted value. As indicated before, the uncertainty in each rate value originates from the complete range (or spread) of rate constant values that permitted satisfactory ACUCHEM analysis of each set of experimental measurements. These uncertainties, following the Debye−Hückel relation, appropriately reduce in magnitude for the $I \rightarrow 0$ condition but continue to represent the real experimental uncertainties in each case. Thus, in each case these rate values with their associated actual experimentally derived uncertainties have been retained over the average value. Possible reasons may be (a) incorporation of H-atom reactions instead of following the general practice of ignoring these (in oxidative studies), especially in acidic pH, and (b) higher accuracy (and

TABLE 6: Results from This Study and Selected Rates for Other Reactions of Scheme 1[a]

reactions	rate constant[b] (M^{-1} s^{-1})
$SO_3^{\bullet-} + O_2 \rightarrow SO_5^{\bullet-}$	1.1×10^9 (recommended; see Appendix A)
$SO_5^{\bullet-} + SO_5^{\bullet-} \rightarrow 2SO_4^{\bullet-} + O_2$	$(2.2 \pm 0.3) \times 10^8$
$SO_5^{\bullet-} + SO_5^{\bullet-} \rightarrow S_2O_8^{2-} + O_2$	$(2.1 \pm 0.3) \times 10^8$
$SO_5^{\bullet-} + HSO_3^- \rightarrow HSO_4^- + SO_4^{\bullet-}$	$(6.0 \pm 0.4) \times 10^7$
$SO_5^{\bullet-} + SO_3^{2-} \rightarrow HSO_4^- + SO_4^{\bullet-}$	$(5.6 \pm 0.6) \times 10^8$
$SO_5^{\bullet-} + HSO_3^- \rightarrow HSO_5^- + SO^{3\bullet-}$	$(3.0 \pm 0.3) \times 10^7$
$SO_5^{\bullet-} + SO_3^{2-} \rightarrow SO_5^{2-} + SO_3^{\bullet-}$	$(1.0 \pm 0.1) \times 10^8$
$SO_3^{\bullet-} + HSO_5^- \rightarrow HSO_3^- + SO_5^{\bullet-}$	$(1.3 \pm 0.1) \times 10^4$ (calcd from ΔE in ref 7 and k_f above)
$SO_3^{\bullet-} + SO_5^{2-} \rightarrow SO_5^{\bullet-} + SO_3^{2-}$	$(4.3 \pm 0.4) \times 10^6$ (as above)
$SO_4^{\bullet-} + HSO_5^- \rightarrow SO_5^{\bullet-} + HSO_4^-$	$(1.0 \pm 0.10 \times 10^6$ (previous result modified)
$SO_4^{\bullet-} + SO_5^{2-} \rightarrow SO_5^{\bullet-} + SO_4^{2-}$	$(1.0 \pm 0.2) \times 10^8$
$H^\bullet + HSO_5^- \rightarrow SO_4^{\bullet-} + H_2O$	$(8.0 \pm 0.7) \times 10^7$
$^\bullet OH + HSO_5^- \rightarrow SO_5^{\bullet-} + H_2O$	$(5.0 \pm 0.3) \times 10^6$ (previous result modified)
$SO_5^{\bullet-} + S_2O_6^{2-} \rightarrow SO_4^{\bullet-} + S_2O_7^{2-}$	$\sim 10^7$ (see Appendix A for details)
$SO_4^{\bullet-} + SO_4^{\bullet-} \rightarrow S_2O_8^{2-}$	$(7.0 \pm 0.6) \times 10^8$ (calcd from ref 9 values; see Appendix A for details)
$SO_4^{\bullet-} + HSO_3^- \rightarrow SO_3^{\bullet-} + HSO_4^-$	$(7.0 \pm 0.6) \times 10^8$ (best from previous estimates)
$SO_4^{\bullet-} + SO_3^{2-} \rightarrow SO_3^{\bullet-} + SO_4^{2-}$	$(1.1 \pm 0.1) \times 10^9$ (as above)

[a] $SO_5^{\bullet-}$ radical absorption: $\lambda_{max} = 260-265$ nm; $\epsilon(260-265\ nm) = 1065 \pm 80\ M^{-1}\ cm^{-1}$. [b] For $I \rightarrow 0$.

ease) of matrix preparations in acid pH. In Table 6, additionally other rate constants that have been modified, calculated, or selected (Appendix A) from other studies are also included for the sake of completion. For future modeling or simulation of atmospheric S(IV) chain oxidation, these values are recommended. However, at this stage, it is to be noted that these results at 25 °C may not always present a complete picture of chemistry in atmospheric liquid hydrometeors. Since wide fluctuations in ambient temperatures are common phenomena, representative modeling of atmospheric sulfuric acid generation in liquid hydrometeors would be closer to reality only after the variations of ambient temperature are suitably incorporated in the models.

Acknowledgment. I thank Dr. Pedatsur Neta and Dr. Robert E. Huie for valuable comments and helpful suggestions during the course of this study and Dr. Tulsi Mukherjee for a preview of the manuscript. I sincerely appreciate the magnanimous comments offered by the reviewers.

Appendix A

A few examples of selected rate constants are as follows.

(1) Addition of O_2 to $SO_3^{\bullet-}$ radical. More recent data of Buxton et al.[10] provides a value of $2.5 \times 10^9\ M^{-1}\ s^{-1}$ from PR measurement in the presence of SO_3^{2-} and O_2. As discussed later in the text, the inherent complexity of reactions in this matrix and incorrect projections of their reaction scheme for kinetic analysis lend incomplete support for this value. Instead, the rate constant $1.1 \times 10^9\ M^{-1}\ s^{-1}$ proposed by Huie et al.[37] was obtained from LFP of $S_2O_6^{2-}$ in the presence of O_2 following a simple reaction scheme without any significant interference from any solute or radical in the matrix. Although we have not been able to arrive at a final estimate of the reaction 8 rate, a limiting value of $\sim 10^7\ M^{-1}s^{-1}$ was obtained from preliminary experiments with the $SO_5^{\bullet-}$ radical in the presence of $S_2O_6^{2-}$. Therefore, interference of reaction 8 in LFP experiments is expected to be low in the time scale of the $SO_3^{\bullet-} + O_2$ reaction. In this context, a possible explanation for the first-order kinetics at 450 nm observed by Huie et al.[37] is that it probably originated as a result of oversimplification of an actual complex kinetics of simultaneous formation and decay of the $SO_4^{\bullet-}$ radical.

(2) Reactions between the $SO_4^{\bullet-}$ radical and the solutes HSO_3^-/SO_3^{2-}. A survey of the database reveals rate values ranging between 4×10^8 and $20 \times 10^8\ M^{-1}\ s^{-1}$. The selected values in our study were taken from the works of Wine et al.[46] and Neta and Huie.[47] However, an opposite trend of rate constant values proposed by Hayon et al.[12] could not be confirmed in our study and was not considered further.

(3) Radical dimerization reaction of the $SO_4^{\bullet-}$ radical. The reaction plays an important role in our study, and its value of $(7.0 \pm 0.6) \times 10^8\ M^{-1}s^{-1}$ for $I \rightarrow 0$ was arrived at by extrapolating the literature decay rates (NIST database[9]) at the reported ionic strengths and by using the latest ϵ values from Buxton et al.[10] for the $SO_4^{\bullet-}$ radical absorptions at the wavelengths reported in these measurements. Similarly, for the reaction of H_2O with the $SO_4^{\bullet-}$ radical the more recent value of $\sim 9.3\ M^{-1}\ s^{-1}$ from the database was used.

Appendix B

Although the yields of radiolytically produced radicals, ions and molecular species in aqueous solutions at 10^{-7} s are well established,[23] the after-pulse concentrations of these and other species arising out of solute reactions change in some cases. These changes are expected when the electron-beam pulse widths are greater than 10^{-7} s. For example, in our experiments, to get a dose of more than 16 Gy, the 520 ns and 2.2 μs pulses (beam fwhm) were needed. Various rate constant values in different tables suggest that partial radical−solute and radical−radical reactions are possible even within the pulse duration.

Therefore, the prevailing after-pulse concentrations of different species were first obtained from ACUCHEM analyses of their generations (proportional to individual G values and the dose rate) and reactions for the duration of the pulse. The actual pulse profile (duration) was divided into sections of narrower widths ($\leq 10^{-7}$ s), and a similar approach was adopted for each section separately and sequentially. For example, the dose rate for each section was equal to the fraction of the total dose {=(total dose × area of pulse profile in this section/total pulse profile area)/section time width in s}. Concentrations of various species at the end of the first section were used as the starting concentrations for the next section. We found that, instead of assuming a square pulse shape for the electron beam, use of the actual pulse shape for these calculations produced better results. This happened because the beginning, some middle, and also the end sections of the pulse had irregular curved profiles. A few examples are as follows.

(1) For a 48 Gy 520 ns pulse in N_2O saturated pH 10.5 solution of 2.5 mM SO_5^{2-} and 100 μM SO_3^{2-}, the concentrations of various species (in μM) are $SO_5^{\bullet-} = 15.7$, $SO_3^{\bullet-} = 0.034$, $SO_4^{\bullet-} = 0.18$, $^\bullet OH = 9.3$, $H_2O_2 = 3.6$, $H^\bullet = 2.9$, $HO_2^\bullet = 0.1$, $O_2^{\bullet-} = 0.023$, remaining $SO_3^{2-} = 99.7$, and $SO_5^{2-} = 1980$.

(2) For a 102 Gy 2.2 μs pulse in N_2O (12.5 mM) and O_2 (0.64 mM) bubbled 0.65 mM HSO_3^- solution at pH 4.0, the concentrations of various species (in μM) are $SO_4^{\bullet-} = 0.37$, $SO_3^{\bullet-} = 21$, $^\bullet OH = 17.6$, $SO_5^{\bullet-} = 9.2$, $H_2O_2 = 9.2$, $H^\bullet = 0.065$, $HO_2^\bullet = 8.3$, $O_2^{\bullet-} = 1.17$, $O_3^{\bullet-} + HO_3^\bullet = 0.4$, and remaining $HSO_3^- = 630$.

In the figures representing cases where such steps were followed, the time window covering the pulse width is shaded.

Appendix C

In the first analysis of $SO_5^{\bullet-}$ radical decay in acid pH described above, the literature value for reaction 12 was used. The resulting k_2 and k_5 were used next in the analysis of reaction 12 here, and the resulting *redefined* k_{12} was again used for

analysis of $SO_5^{\bullet-}$ radical decay in the next section. This cycle was repeated until further change in results in either analysis became negligible. Thus, the k_2 and k_5 values described and used in this analysis represent the final set from the next section. Effect of solution ionic strength was appropriately followed in every step. During analysis of other related rates, a similar approach was essential.

References and Notes

(1) Bigelow, S. L. *Z. Phys. Chem.* **1898**, *28*, 493. Young, S. W. *J. Am. Chem. Soc.* **1902**, *24*, 297. Titoff, A. *Z. Phys. Chem.* **1903**, *45*, 641. Bäckström, H. L. J. *J. Am. Chem. Soc.* **1927**, *49*, 1460. Alyea, H. N.; Bäckström, H. L. J. *J. Am. Chem. Soc.* **1929**, *51*, 90.

(2) Zellner, R.; Herrman, H. Free Radical Chemistry of the Aqueous Atmospheric Phase. In *Spectroscopy in Environment Science*; Clark, R. J. H., Hester, R. E., Eds.; John Wiley & Sons Ltd.: New York, 1995; pp 381−451.

(3) Ravishankara, A. R. *Science* **1997**, *276*, 1058.

(4) Calvert, J. G.; Lazrus, A.; Kok, G. L.; Heikes, B. G.; Walega, J. G.; Lind, J.; Cantrell, C. A. *Nature* **1985**, *317*, 27.

(5) Rudich, Y.; Talukdar, R. K.; Ravishankara, A. R. *J. Geophys. Res. D* **1998**, *103*, 16133.

(6) van den Berg, A.; Dentner, F.; Lelieveld, J. *J. Geophys. Res. D* **2000**, *105*, 11671.

(7) Das, T. N.; Huie, R. E.; Neta, P. *J. Phys. Chem. A* **1999**, *103*, 3581.

(8) Wardman, P. *J. Phys. Chem. Ref. Data* **1989**, *18*, 1637.

(9) Ross, A. B.; Bielski, B. H. J.; Buxton, G. V.; Greenstock, C. L.; Helman, W. P.; Huie, R. E.; Grodkowski, J.; Neta, P.; Mallard, W. G. *NDRL-NIST Solution Kinetics database*, Version 3; NIST Standard Reference Database 40; National Institute of Standards and Technology: Gaithersburg, MD, 1994.

(10) Buxton, G. V.; McGowan, S.; Salmon, G. A.; Williams, J. E.; Wood, N. D. *Atmos. Environ.* **1996**, *30*, 2483.

(11) Huie, R. E.; Neta, P. *Atmos. Environ.* **1987**, *21*, 1743.

(12) Hayon, E.; Trenin, A.; Wilf, J. *J. Am. Chem. Soc.* **1972**, *94*, 47.

(13) Huie, R. E.; Clifton, C. L. Altstein, N. *Radiat. Phys. Chem.* **1989**, *33*, 361.

(14) Deister, U.; Warneck, P. *J. Phys. Chem.* **1990**, *94*, 2191.

(15) Yermakov, A. N.; Zhitomirsky, B. M.; Poskrebyshev, G. A.; Sozurakov, D. M. *J. Phys. Chem.* **1993**, *97*, 10712.

(16) Herrman, H.; Reese, A.; Zellner, R. *J. Mol. Struct.* **1995**, *348*, 183.

(17) Pandis, S. N.; Seinfeld, J. H. *J. Geophys. Res. D* **1989**, *94*, 1105.

(18) van Eldik, R.; Harris, G. M. *Inorg. Chem.* **1980**, *19*, 880. Smith, R. M.; Martell, A. E. *Critical Stability Constants, Inorganic Complexes*; Plenum: New York, 1976; Vol. 4.

(19) Guha, S. N.; Moorthy, P. N.; Kishore, K.; Naik, D. B.; Rao, K. N. *Proc. Indian Acad. Sci. (Chem. Sci.)* **1987**, *99*, 261.

(20) Das, T. N. *J. Phys. Chem. A* **1998**, *102*, 426.

(21) Buxton, G. V.; Stuart, C. R. *J. Chem. Soc., Faraday Trans.* **1995**, *91*, 279.

(22) W. Braun, W.; Herron, J. T.; Kahaner, D. *Int. J. Chem. Kinet.* **1988**, *20*, 51.

(23) Buxton, G. V.; Greenstock, C. L.; Helman, W. P.; Ross, A. B. *J. Phys. Chem. Ref. Data* **1988**, *17*, 513.

(24) Domae, M.; Katsumura, Y.; Ishigure, K.; Byakov, V. M. *Radiat. Phys. Chem.* **1996**, *48*, 487.

(25) Maruthamuthu, P.; Neta, P. *J. Phys. Chem.* **1977**, *81*, 937.

(26) Roebke, W.; Renz, M.; Henglein, A. *Int. J. Radiat. Phys. Chem.* **1969**, *1*, 39.

(27) Hug, G. L. *Optical Spectra of Nonmetallic Inorganic Transient Species in Aqueous Solution*; NSRDS-NBS 69; U.S. Department of Commerce; Washington, DC, 1981.

(28) Matthews, R. W.; Mahlman, H. A.; Sworski, T. J. *J. Phys. Chem.* **1970**, *74*, 2475.

(29) Simic, M.; Neta, P.; Hayon, E. *J. Phys. Chem.* **1969**, *73*, 3794.

(30) Ye, M.; Schuler, R. H. *Radiat. Phys. Chem.* **1986**, *28*, 223.

(31) Maruthamuthu, P.; Neta, P. *J. Phys. Chem.* **1978**, *82*, 710.

(32) Klaning, U.K.; Sehested, K.; Appelman, E. H. *Inorg. Chem.* **1991**, *30*, 3582.

(33) Schuler, R. H.; Hartzell, A. L.; Behar, B. *J. Phys. Chem.* **1981**, *85*, 192.

(34) Büehler, R. E.; Staehelin, J.; Hoigne, J. *J. Phys. Chem.* **1984**, *88*, 2560.

(35) McElroy, W. J.; Deister, U. *National Power Research Report*; ESTB/L/0173/R90; 1990. Jacob, D. J. *J. Geophys. Res.* **1986**, *91*, 9807.

(36) Jayson, G. G.; Parsons, B. J.; Swallow, A. J. *J. Chem. Soc., Faraday. Trans. 1* **1973**, *69*, 1597.

(37) Huie, R. E.; Clifton, C. L.; Neta, P. *Radiat. Phys. Chem.* **1991**, *38*, 477.

(38) Klaning, U. K.; Wolff, T. *Ber Bunsen-Ges. Phys. Chem.* **1985**, *89*, 243.

(39) Wu, D.; Wong, D.; DiBartolo, B. *J. Photochem.* **1980**, *14*, 303.

(40) Neta, P.; Huie, R. E. *J. Phys. Chem. Ref. Data* **1988**, *17*, 1027.

(41) Mozurkewich, M. *J. Geophys. Res.* **1995**, *100*, 14199.

(42) Martin, L. R. In *Acid Precipitation Series*; Calvert, J. G., Ed.; Butterworth: Boston, 1994; Vol. 3, pp 63−100.

(43) Warneck, P. *Chemistry of the Natural Atmosphere*; Int. Geophys. Series, Academic Press: San Diego, 1988; pp 404−418. Charlson, R. J.; Rohde, H. *Nature* 1982, *195*, 683.

(44) Neta, P.; Huie, R. E. *J. Phys. Chem.* **1985**, *89*, 1 783.

(45) Warneck, P. *Ber. Bunsen-Ges. Phys. Chem.* **1992**, *96*, 454.

(46) Wine, P. H.; Tang, Y.; Thorn, R. P.; Wells, J. R.; Davis, D. D. *J. Geophys. Res. D* **1989**, *94*, 1085.

(47) Neta, P.; Huie, R. E. *J. Phys. Chem.* **1986**, *90*, 4644.

(48) Zehavi, D.; Rabani, J. *J. Phys. Chem.* **1971**, *75*, 1738.

(49) Thomas, J. K. *Trans. Faraday Soc.* **1965**, *61*, 702.

(50) Christensen, H.; Sehested, K.; Bjergbakke, E. *Water Chem. Nucl. React. Syst.* **1989**, *5*, 141.

(51) Ellit, A. J.; Buxton, G. V. *J. Chem. Soc., Faraday Trans.* **1992**, *88*, 2465.

(52) Feng, P. Y.; Brynjolfsson, A.; Halliday, J. W.; Jarrett, R. D. *J. Phys. Chem.* **1970**, *74*, 1221.

(53) Czapski, G.; Peled, E. *Isr. J. Chem.* **1968**, *6*, 421.

(54) Christensen, H.; Sehested, K.; Logager, T. *Radiat. Phys. Chem.* **1994**, *43*, 527.

(55) Bielski, B. J. H.; Cabelli, D. E., Arudi, R. L.; Ross, A. B. *J. Phys. Chem. Ref. Data* **1985**, *14*, 1041.

(56) Marsh, C.; Edwards, J. O. *Proj. React. Kinet.* **1989**, *15*, 35.

(57) Buxton, G. V.; Salmon, G. A.; Wood, N. D. *Proc. 5th Eur. Symp. Phys.-Chem. Behav. Atmos. Pollut.*; Restelli, G., Angeletti, G., Eds.; Kluwer: Dordrecht, The Netherlands, 1989−90; p 245.

(58) Yermakov, A. N.; Zhitomirsky, B. M.; Poskrebyshev, G. A.; Stoliarov, S. I.; *J. Phys. Chem.* **1995**, *99*, 3120.

(59) Jiang, P.-Y.; Katsumura, Y.; Nagaishi, R.; Domae, M.; Ishikawa, K.; Ishigure, K.; Yoshida, Y. *J. Chem. Soc., Faraday Trans.* **1992**, *88*, 1653.

(60) McElroy, W. J. *J. Phys. Chem.* **1990**, *94*, 2435.

(61) Grigor'ev, A. E.; Makarov, I. E.; Pikaev, A. K. *High Energy Chem.* **1987**, *21*, 99.

(62) Nagarajan, V.; Fessenden, R. W. *J. Phys. Chem.* **1985**, *89*, 2330.

(63) Navaratnam, S.; Parsons, B. J.; Swallow, A. J. *Radiat. Phys. Chem.* **1980**, *15*, 159.

(64) Huie, R. E.; Clifton, C. L. *J. Phys. Chem.* **1990**, *94*, 8561.